Aerosol Science and Engineering
https://doi.org/10.1007/s41810-025-00372-7

ORIGINAL PAPER

Enhancing the $PM_{2.5}$ Predictions of US Embassies Using Novel Hybrid 1DCNN-BiGRU and Decomposed-Recomposed 1DCNN-BiGRU-DR Models

Naushad Ahmad[1] · **Vipin Kumar**[1]

Received: 2 September 2024 / Revised: 3 August 2025 / Accepted: 7 December 2025

Abstract
Air pollution is a worldwide crisis that contributes to numerous human problems related to environmental and public health. $PM_{2.5}$ pollution concentration is one of the major contributors to air pollution. $PM_{2.5}$ is known to penetrate deep into the respiratory system upon inhalation, leading to a wide range of health problems, such as respiratory infections, cardiovascular diseases, and even premature death. This study used the AirNow platform to obtain various US Embassies and consolates $PM_{2.5}$ data in the Indian subcontinent and China. The article proposed two hybrid models to enhance the performance of the model's accuracy. The prop-1 hybrid model is a one-dimensional convolutional neural network and a bidirectional gated recurrent unit (1DCNN-BiGRU), using their abilities to capture spatial and temporal dependencies in $PM_{2.5}$ data. The prop-2 (1DCNN-BiGRU-DR) model further enhances the accuracy with the Decomposed-Recomposed (DR) techniques. The DR technique also enhances the model's capacity to capture complex spatiotemporal patterns inherent in the data. The comparison of the suggested model with conventional deep learning models is conducted to assess a variety of parameter measures, including statistical and non-statistical parameters and graphical analysis. The assessment metrics, which include mean absolute error (MAE), root mean square error (RMSE), mean absolute percentage error (MAPE), and mean square logarithmic error (MSLE), illustrate the efficacy of the proposed models. Three distinct analysis patterns were pursued: Prop-1 vs. DL, Prop-2 vs. DL, and Prop-2 vs. DL-DR. The performance accuracy of Prop-1 is reflected in RMSE: 4.26 ± 0.12, and MAE: 2.27 ± 0.08. Similarly, the performance accuracy of Prop-2 is demonstrated by RMSE: 4.18 ± 0.10, and MAE: 2.44 ± 0.09. RMSE ranking across all three proposed model analyses secured the first rank, demonstrating superior predictive performance. The proposed models got superior results compared to the AIC-BIC test, Friedman ranking, Diebold Mariano test, and Taylor diagram evaluation. Results indicate that the prop-1 model integrated with the decompose-recompose methodology outperforms traditional deep learning methods, exhibiting superior prediction accuracy across multiple embassy locations. This study significantly contributes to the progression of forecasting methods for air quality on Earth. It has tangible implications for creating comprehensive and practical strategies that promote the well-being of individuals and the environment.

Keywords Time series forecasting · Earth air quality · Deep learning · $PM_{2.5}$ · Decomposition-recomposition · Hybrid time series model

1 Introduction

Today, no one is untouchable from climate change and its impact on our environmental life and the layers of the atmosphere. Almost every developed and developing country is facing the issue of climate change. Climate change and its effect on the earth's environment are not new issues. The issue has persisted for an extended period. The problem remains unresolved at present. Climate change is a

✉ Vipin Kumar
rt.vipink@gmail.com

Naushad Ahmad
naushad13bhu@gmail.com

[1] Computer Science and Information Technology, Mahatma Gandhi Central University, Motihari, Bihar 845401, India

Published online: 16 January 2026

long process. Solving the same problem could take a long time. The increase in global temperatures is because of the greenhouse gases increasing in the Earth's atmosphere and, consequently, global glaciers melting. Most of human civilization is going to face natural disasters. They live in coastal regions and mountains. The Environmental Protection Agency (EPA) received modeling assistance from California State University (Limperis et al. 2023). Assessing air pollution is critical, and the EPA recommends $PM_{2.5}$ as a key parameter for individuals with varying health levels. To limit climate change, the global conference named CoP (Conference of Parties) reviews and actions taken by the communities constituted by the United Nations Framework Convention on Climate Change (UNFCCC) every year (Hickmann et al. 2021). The main aim of the UNFCCC is to focus on climate change. It recognizes the close link between air pollution and climate change. The process of forming pollution particles combines aerosol and dust particles. Some hazardous pollutants are $PM_{2.5}$, PM_{10}, NO_2, SO_2, CO, and O_3(ozone) (Sethi and Mittal 2021). Each air pollution concentration has different characteristics and is associated with different health problems. One major pollutant is particulate matter with an aerodynamic diameter between (0.1 to 10) micrograms per cubic meter. Air pollution disturbs human health and ecosystems globally. $PM_{2.5}$ is the most dangerous substance for human health. The $PM_{2.5}$ fine inhalable particles. For perspective, a single hair from your head is about 70–80 (μm) micrometers in diameter, making it 30–32 times larger than the largest fine particle. Some particles less than 10 (μm) micrometers in diameter can penetrate and lodge deep within your lungs, and some may even get into your bloodstream (Stafoggia et al. 2019). $PM_{2.5}$ concentration is the most dangerous for infants and older adults. Infants and children are victims of $PM_{2.5}$ concentrations. Children are in hazardous zones because they have a low tendency to tackle high concentrations of pollution compared to adults. So many diseases are listed in research papers due to increases in $PM_{2.5}$ concentrations. Short-term exposure to $PM_{2.5}$ concentration has caused eye irritation, sneezing, headache, irritation, and among others. Some of the significant health issues or long-term exposure to air pollution concentration are asthma, respiratory inflammation, arrhythmias (irregular heartbeats), wheezing (trouble breathing), coughing, and Chronic obstructive pulmonary disease (COPD) (Mohan and Abraham 2024). COPD is a group of diseases related to respiratory systems that block the airflow in and out of the lungs.

WHO air quality guidelines aim to protect millions of lives from air pollution by reducing air pollution and mitigating climate change to help protect our health. Recent studies noted that COPD mainly causes 16% of total deaths worldwide (Islam et al. 2023). The WHO reports that chronic lung and heart diseases are responsible for approximately 4 million deaths worldwide each year due to air pollution. According to this study, 2.49 million people died due to lower respiratory tract infections in 2019, making it the fourth leading cause of death worldwide (Hu et al. 2023b). Recently (Yu et al. 2024) studied that the effect from 1990 to 2019 reveals a correlation between low temperatures and the global burden study of LRI. Most of these premature deaths occurred in Asia, Africa, and Europe (AAE), accounting for 3148.3, 383.4, and 388.3 thousand deaths, or 96% of the global total, respectively. In these studies (Cebrián et al. 2022) and Zhu and Shi (2023), results show that air pollution hurts global health and requires immediate action. High pollution and densely populated areas have led to millions of deaths in the Asia-Pacific alone (Hari Prasad Peri 2023). Air pollution sources can be quite different from each other and may have considerable and varying health consequences.

The "State of India's Environment Report" published a report on death showing that 6.67 million people died due to air pollution worldwide, and 1.67 million premature deaths happened in India in 2019 (Hu et al. 2023a). The air pollution situation in India is alarming, with a growing number of cities experiencing severe pollution. In the last two decades, the death rate has increased by 2.5 times. The Global Burden of Disease (GBD) research estimates that ambient $PM_{2.5}$ pollution contributed to 1.4 million of China's premature deaths in 2019 (Zhou et al. 2024). The study conducted in 2019 focused on the GBD caused by ambient particulate matter pollution in respiratory diseases (Wu et al. 2021). Air pollution made up about 14% of China's total fatalities. Beijing's annual mean $PM_{2.5}$ concentration in 2020 was 38 $\mu g/m^3$, four times higher than the WHO 2019 limit of 10 $\mu g/m^3$. This pollution level exceeded the 2012-introduced Level 2 China Ambient Air Quality Standards (> 35 $\mu g/m^3$) (Geng et al. 2021). Air pollution is the 6th leading risk factor for mortality in Pakistan, accounting for more than 9% of deaths (128,000), according to the data on the state of the global air presented in 2019 (Bilal et al. 2021). In Bangladesh, air pollution is estimated by the World Bank to have contributed to 78,145–88,229 premature deaths in 2019. This represents 20% of the country's total deaths and 4–5 % of GDP (Raza et al. 2022).

To improve air quality because 9 out of 10 people suffer from poor air quality. The authors have designed and developed a model to predict and forecast air quality for the future. After creating the best model, authors analyze and take care of our health in the future. Today's air quality modeling also protects our health from lousy air quality. Sometimes, a single person can protect yourself from air pollution, but the whole community cannot. The authors design a centralized model to predict air quality in the Asian-pacific

region. The utilization of the spatio-temporal domain is considered a potential solution for improving prediction accuracy (Sharma et al. 2024). Air pollution modeling is crucial in finding the complex relationship between pollutants' spatial and temporal distribution across different areas and population groups (Kotsev et al. 2015). Researchers utilized air pollution modeling techniques for data assimilation to enhance our ability to predict accurately. Addressing air pollution requires emphasizing action as the focal point and assessing air quality and emissions from activities like coal transportation via trucks, where coal dust has been validated as a significant source of visible dust particles (Choi et al. 2022).

Deep Learning (DL) has emerged as a powerful tool for modeling complex spatiotemporal relationships in environmental data. Now emphasize the complexity of $PM_{2.5}$ patterns, which vary both over time and across locations, justifying the need for models capable of capturing both temporal dependencies (via BiGRU) and local spatial trends (via 1DCNN). The findings (Shekdar 2009) revealed executing effective waste management strategies, deploying methods to reduce dust in construction activities, enacting legislation concerning air quality, and formulating comprehensive strategies. One of the solutions to minimize indoor air pollution is to plant more air purifier plants, but they work only around us. Authorities should develop a series of potential measures, considering the diverse sources of air pollution and their varying health implications. Solutions may include transitioning to clean energy, improving vehicle emissions standards, enhancing public transportation, implementing industrial emission controls, promoting sustainable agriculture and urban planning strategies, encouraging energy efficiency, raising public awareness, strengthening air quality monitoring, and fostering international cooperation to tackle this multifaceted environmental issue (Khanam et al. 2023). The impact of air pollution motivates us to work in the broader environment to reduce the effect of pollution on human health and secure our environment. The proposed model is a hybrid approach that demonstrates high accuracy in predicting $PM_{2.5}$ air pollution levels.

The Air Quality Index (AQI) shows air quality on a 0–500 scale. It simplifies complicated data on different pollutants' air quality into a single number, terminology, and color. The Table 1 compares annual and 24-hour average thresholds across countries and international organizations of ambient air quality standards to particulate matter. The USNAAQS establishes a rigorous yearly average of 12 $\mu g/m^3$, contrasting to Bangladesh's BNAAQS of 15 $\mu g/m^3$" for the identical parameter. The real-world data from US embassy measurements reveal alarming exceedances, with India's National Ambient Air Quality Standard (NAAQS) $PM_{2.5}$ levels surpassing its standards by 107.56%, highlighting widespread air pollution challenges. Moreover, Pakistan National Environmental Quality Standards (NEQS) and Bangladesh exhibit staggering exceedance percentages of 178.57% and 450.57%, respectively. This table analysis underscores the urgent need for comprehensive strategies to mitigate global air pollution's adverse impacts on health and environmental sustainability, particularly emphasizing high-exceedance regions. WHO air quality guidelines reduced the annual average standard of $PM_{2.5}$ because of the limited values for specific air pollutants to help countries protect public health. In the conclusion of the table analysis, replicate the real-world data and lots of the reports published that 99 out of the world's 100 most polluted cities are in Asian continents, with 83 of them in India.

The $PM_{2.5}$ data were obtained from the AirNow platform,[1] which provides real-time and historical air quality measurements from US embassies worldwide.

The $PM_{2.5}$ air pollution data from AirNow at US Embassies and Consulates in the Indian subcontinent and China, shown in Fig. 1. The researcher worked on collecting four embassies and seven consulates air pollution $PM_{2.5}$ data, which authors collectively called the embassies dataset. The

Table 1 Ambient air quality standards versus real-world observations for $PM_{2.5}$ pollution time weighted average, US embassy annual mean and exceeded percentage (2019–2023)

Standard[a]	Annual Average	24-Hour Average	Country	US Embassy Annual Mean	Exceeded Percentage	Pollution Rank[b]
USNAAQS	12 $\mu g/m^3$	35 $\mu g/m^3$	US	–	–	None
INAAQS	40 $\mu g/m^3$	60 $\mu g/m^3$	India	83.02 $\mu g/m^3$	107.56%	3
NEQS	15 $\mu g/m^3$	35 $\mu g/m^3$	Pakistan	41.78 $\mu g/m^3$	178.57%	2
CNAAQS	35 $\mu g/m^3$	75 $\mu g/m^3$	China	35.58 $\mu g/m^3$	1.66%	4
BNAAQS	15 $\mu g/m^3$	65 $\mu g/m^3$	Bangladesh	82.58 $\mu g/m^3$	450.57%	1
AQGs	5 $\mu g/m^3$	15 $\mu g/m^3$	WHO	–	–	None

[a]Standards: USNAAQS—United States National Ambient Air Quality Standards; INAAQS—Indian NAAQS; NEQS—National Environmental Quality Standards (Pakistan); CNAAQS—Chinese NAAQS; BNAAQS—Bangladesh NAAQS; AQGs—WHO Air Quality Guidelines

[b]Pollution Rank: Computed by authors using 5-year mean $PM_{2.5}$ values (2019–2023) from the AirNow platform

[1] https://www.airnow.gov/

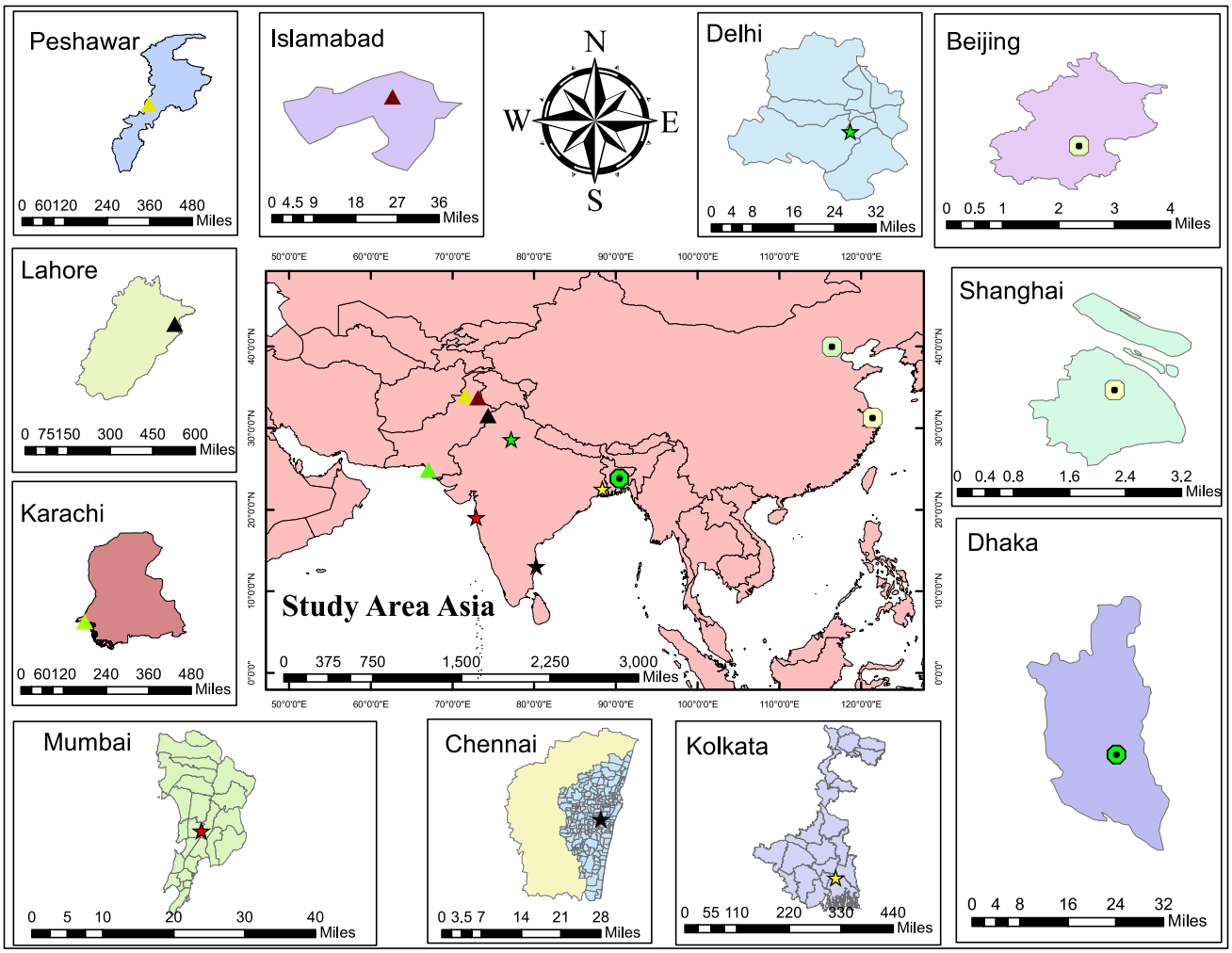

Fig. 1 The research focuses on the geographic distribution of US embassies and consulate locations along with $PM_{2.5}$ air pollution monitoring stations

dataset used in this study covers the period from 15 May 2019 to 28 January 2023. Some consulates are removed because they have a negative correlation with each other. Only positive correlations are taken to utilize our proposed air pollution modeling in this correlation figure. This study investigates the use of traditional deep learning models with decomposed and recomposed techniques. Decomposition involves separating datasets into simpler components like residuals, seasonal, and trends. The sum of all three gives the actual form of the dataset. That means the authors divided the whole dataset into three different datasets. Each dataset has distinct characteristics. Residual and seasonal values have positive and negative values, but the trend only has positive values. The actual air pollution dataset has only positive values because air pollution can not be in negative form. In this paper, our main objective is to propose a hybrid 1DCNN-BiGRU model utilizing the decompose and recompose technique to improve the predictive capabilities. This hybrid architecture combines the strengths of both convolutional and bidirectional GRU layers to capture spatial and temporal dependencies in sequential data effectively.

The following summarises the primary contributions of this study:

- The collection of the datasets from the AirNow website to the various U.S. Embassies and consulates of the Indian subcontinent and China.
- The prop-1 (1DCNN-BiGRU) model effectively combines the strengths of both convolutional and recurrent networks, enabling it to achieve higher predictive accuracy compared to traditional deep learning models.
- The prop-2 (1DCNN-BiGRU-DR) model is accurately forecast when authors compared it to the traditional DL models and traditional DL-DR over various evaluation parameters.
- The prop-1 (1DCNN-BiGRU) and prop-2 (1DCNN-BiGRU-DR) models have been compared with

state-of-the-art forecasting models likes LSTM, BiLSTM, GRU, RNN, and CNN over RMSE, MAE, MAPE, and MSLE.
- The performance of prop-1 and prop-2 have been statistically validated using Friedman Ranking, Diebold Mariano test, AIC-BIC test, and Taylor Diagram.

The organization of the paper is as follows. Sect. 2 provides a comprehensive review of the related literature and outlines the research gaps. Sect. 3 contains the 3.1 subsection study area and data collection. The subsect. 3.2 of EDA contains the statistical analysis, decomposition and autocorrelation function analysis, and spatio-temporal correlation analysis. In Sect. 4, deep learning models contain the BiGRU, 1DCNN, LSTM, and RNN. The Sect. 5 contains two subsections of the proposed-1 model and proposed-2 model. In Sect. 6, the experimental setup contains the subsect. 6.1 Parameters setting of deep learning models, and subsect. 6.2 hardware and software required. The Sect. 7 contains the subsect. 7.1 quantitative analysis, 7.2 graphical analysis, 7.3 statistical analysis of results. The last Sect.8 contains the conclusion of the research.

2 Literature Review

Accurately predicting $PM_{2.5}$ concentrations is crucial due to its harmful impact on human health, as highlighted in Table 2 Various advanced methods have been proposed for $PM_{2.5}$ prediction, such as combining the hybrid algorithm of autoregressive integrated moving average and adaptive-neuro fuzzy inference system (Yang et al. 2022), weighted complementary ensemble empirical mode decomposition with adaptive noise and improved long- and short-term memory ILSTM neural network (Xie et al. 2023), and utilizing deep learning with GRU for accurate predictions. The literature overviews recent air quality prediction advancements from various studies using different modeling techniques. References like Samad et al. (2023); Prasad et al. (2023); Vignesh et al. (2023) indicate the popularity of machine learning for complex air quality data analysis. Studies in locations like Karlsruhe, Taiwan, with open datasets emphasize the importance of model selection and data quality for accurate predictions. Ensemble techniques, shown by Chen et al. (2023), combine models to enhance performance. The literature review in Table 2 examines recent air quality prediction advances, drawing from diverse studies. In this references (Mohammadi et al. 2024; Bai and Li 2023; Yang et al. 2022) highlight machine learning's effectiveness in capturing air quality patterns. Studies across regions stress the importance of model selection and data quality. Stacking ensemble methods, like Nair et al. (2023), improve predictive performance by combining models. The size of the dataset plays a major role in air pollution modeling. If the dataset sizes are too small, the model is not trained well. It gives one of the biggest problems in the model fitting (underfit). DL required a huge amount of data for better training in the modeling. In these papers (Chen et al. 2023; Bi et al. 2022; Conibear et al. 2022), and Wang et al. (2022) span of the data is almost for the one year. The study area of all the above-cited papers is mainly in Beijing, China, except for one from Kaohsiung, Taiwan. In the recent literature review, it was observed that several studies, such as those by Du et al. (2019), Li (2020), Wu et al. (2023) and Chen et al. (2024) used single-year datasets, all of which were collected from locations in China.

Several research studies, exemplified by Xie et al. (2023) and Li and Huo (2023), have delved into the intricate domain of deep learning, utilizing sophisticated architectures like CNN and LSTM networks to effectively capture the intricate temporal and spatial dependencies present in air quality data. These methodologies have shown significant promise in enhancing the accuracy of air quality predictions and tackling the inherent complexities associated with air pollution dynamics. Hybrid deep learning models have improved the accuracy of air pollution predictions by utilizing various architectural frameworks (Ahmad and Kumar 2025a, b, 2023). Nevertheless, within the realm of these advancements, specific gaps in research have been identified, as highlighted by Conibear et al. (2022) and other researchers, underscoring the ongoing challenges in air quality prediction. These challenges include the imperative necessity for improved generalization of models, the utilization of larger datasets, and the exploration of innovative methodologies to accommodate the dynamic characteristics of air pollutants more effectively. Additionally, various research was conducted by Xie et al. (2023), Li and Huo (2023), and Qing (2023) to predict air pollution in various domains. These methodologies have demonstrated promising outcomes in enhancing the accuracy of air quality predictions and addressing the intrinsic complexities associated with air pollution dynamics. However, despite these advancements, specific gaps in research, as emphasized by Conibear et al. (2022) and Wang et al. (2022), and other scholars, continue to underscore the persistent challenges in air quality prediction.

The common research gap is the utilization of the advanced hybrid model for accurately predicting air pollution $PM_{2.5}$. Some of the literature is utilizing the combing CNN-BiGRU (Li and Huo 2023), stacking ensemble (Nair et al. 2023), AdaBoost (Toharudin et al. 2023), and GRU (Qing 2023) models. In these research articles, the main research gaps require an efficient DL hybrid model, Bai and Li (2023) and Wang et al. (2021) have both implemented DL models. Zamani et al. (2019) implemented machine

Table 2 Recent literature review on the utilization of performance measures and research gap

S. no	References	Data collection or Organization	Span of the data	Model utilization	RMSE, MAE, MSE, R2, MAPE	Research gap
1	Samad et al. (2023)	German city named Karlsruhe	01 January 2018 to 31 March 2022	Machine Learning methods	R2 $\geq$ 0.9	No decomposition used
2	Prasad et al. (2023)	Taiwan Air Quality Monitoring stations	From 2012 to 2017	ANN	R2 = 0.987	No hybrid spatial-temporal modeling
3	Vignesh et al. (2023)	openaq air quality	From 2017 to 2021	RF and SVM	RF (RMSE = 3.121) and SVM (RMSE = 3.125)	No hybrid spatial-temporal modeling
4	Xie et al. (2023)	Beijing air pollutant and meteorological data	01 January 2014 to 05 July 2022	Optimized CNN-LSTM	–	Enhances spatial and temporal characteristics
5	Li and Huo (2023)	New Taipei City, Taiwan	Not described	Combined CNN-BiGRU	RMSE = 8.61	Decomposition not addressed
6	Chen et al. (2023)	Kaohsiung, Taiwan	2021	CNN-RF ensemble framework	RMSE=4.88, MAE=3.3, R2=0.88	Addresses spatial-temporal complexity using a robust hybrid model
7	Wu et al. (2022)	Beijing	1 January 2016 to 31 December 2016	CE-AGA-LSTM	MAE = 14.5 and RMSE = 21.88	Fail to simulate $PM_{2.5}$ dependence on ST
8	Bi et al. (2022)	Central China	02 April 2019 to 10 March 2020	GEOS, RF	R2 = 0.76	Decomposition not addressed
9	Zhang et al. (2020)	China	From 2017 to 2019	XGBoost, RF	RMSE=8.63	Decomposition not addressed
10	Conibear et al. (2022)	China	2015	Machine Learning	RMSE=0.5094, R2=0.9995	Lack of hybrid frameworks
11	Yang et al. (2022)	Beijing-Tianjin-Hebei region	From 2013 to 2020	Statistical regression model	RMSPE 7.87–29.90	Insufficient decomposition techniques
12	Wang et al. (2022)	Beijing	2020	MIFNN, AutoELM	AutoELM (R2=0.80), MIFNN (R2= 0.85)	Limited spatial coverage of $PM_{2.5}$ data
13	Buya et al. (2023)	Thailand	From 2011 to 2020	Machine learning models	R2 = 0.71, RMSE = 8.79	Limited ground station data for $PM_{2.5}$
14	Nair et al. (2023)	Bangalore City	Over 10 years	Stacking Ensemble, XGBoost	Stacking Ensemble (R2= 0.991)	Required hybrid model
15	Toharudin et al. (2023)	Jakarta, Indonesia	From 2015 to 2022	AdaBoost, XGBoost, CatBoost	accuracy between 0.52−0.54	Hybrid model required
16	Shakya et al. (2022)	New Delhi	From 2016 to 2021	LSTM, GRU and ML	R2 values 0.575 to 0.963	LSTM outperformed in PM10 prediction
17	Du et al. (2019))	Beijing air pollution data set from UCI	01 January 2010 to 31 January 2010	DAQFF, CNNs and Bi-LSTM	RMSE=8.20, MAE=6.19	Increase the size of the dataset and required hybrid model
18	Qing (2023)	Changchun observatories	From 2016 to 2020	GRU	RMSE = 18.32, MAE = 13.54	Insufficient decomposition techniques
19	Bai and Li (2023)	Beijing, China	Three years	Deep learning model	RMSE = 17.93 and MAE = 11.52	Advance hybrid model
20	Chae et al. (2021)	Korea Environment Corporation	01 January 2018 to 31 December 2019	ICNN	R-squared $\geq$ 0.97	Increase the size of dataset span
21	Wang et al. (2021)	Beijing, China	01 January 2014 to 31 December 2019	CR-LSTM	R2 = 0.74 and RMSE = 18.96	Insufficient decomposition techniques
22	Xiao et al. (2020)	Beijing–Tianjin–Hebei (BTH) region of China	From 2015 to 2017	WLSTME model integrates MLP, LSTM	RMSE = 40.67 and MAE = 26.10	Required decompose recompose
23	Chen et al. (2021)	National Environmental Monitoring Center	From 2015 to 2017	Deep Bayesian model	R2 = 0.78, RMSE = 19.45	Increase the size of dataset span
24	Li (2020)	U.S. Embassy in Beijing	2015	Robust DL Approach	test R2: 0.90; test RMSE: 22.3	Apply decompose recompose
25	Shao and Kim (2022)	Seoul, South Korea	01 January 2017 to 31 December 2019	CNN-LSTM	RMSE: 8.05, MAE = 5.04, MAPE = 23.96, R2 = 0.7	More data required and utilize decompose recompose

Table 2 (continued)

S. no	References	Data collection or Organization	Span of the data	Model utilization	RMSE, MAE, MSE, R2, MAPE	Research gap
26	Wu et al. (2023)	Beijing-based monitoring sites	1 January 2016 to 31 December 2016	Ensemble Model	MAE = 13.418 and RMSE = 21.401	Advance hybrid model
27	Zamani Joharestani et al. (2019))	Tehran's urban area	–	Random Forest, XGBoost	R2 = 0.81, MAE = 9.93 and RMSE = 13.58	Required hybrid model
28	Natarajan et al. (2024)	India	From 2015 to 2020	DTR, SVR	accuracy=94.25%	Apply DL for better accuracy
29	Mohammadi et al. (2024)	Isfahan, Iran	January 2011 to December 2019	SVM, KNN, RF and ANN	highest accuracy of 91.1%	Required DL hybrid architecture
30	Chen et al. (2024)	Nanjing, China	01 January 2020 to 31 December 2020	L-STCN	R2 = 0.92 and RMSE = 6.75	Increase the size of the data

ANN—Artificial Neural Network; LSTM—Long Short-Term Memory; CNN—Convolutional Neural Network; BiGRU—Bidirectional Gated Recurrent Unit; DR- Decomposed-Recomposed

learning models (Zamani Joharestani et al. 2019). Mohammadi et al. (2024) also implemented machine learning models (Mohammadi et al. 2024). In Xiao et al. (2020) and Li (2020) must apply the decompose recompose technique for the lower RMSE values. These challenges encompass the pressing need for enhanced generalization of models, the utilization of larger datasets, and the exploration of novel methodologies to encapsulate the dynamic nature of air pollutants more effectively. To summarize, integrating these investigations not only emphasizes the progression of air quality forecasting techniques from conventional statistical methods to increasingly complex machine learning and deep learning models but also emphasizes the ongoing necessity of research endeavors to tackle current obstacles and enhance cutting-edge air quality forecasting.

3 Data

Obtained $PM_{2.5}$ air pollution data from US embassies and consulates in the Indian subcontinent and China via AirNow. Initially, a specific city is selected, followed by the selection of a relevant air quality parameter PM2.5 for analysis. All the necessary steps were taken for the preprocessing of the data. Some data are missing in the dataset, and corresponding $PM_{2.5}$ values are also missing. To impute the data in the correct datetime sequence. First, generate the sequence of the date with time. after that, the mean imputation method was applied to all US embassies and consulate datasets.

3.1 Study Area and Data Sources

The geographical locations of all the US Embassies and Consulates included in the study are summarized and visually represented in a single map see Fig. 1. Here, the big map shows the point of the area where US embassies are located, and a corresponding map symbol shows the cities of the exact location on a small map. All Indian cities have four stars with different colors, Pakistani cities have four triangle shapes, China has two square shapes, and Bangladesh has one circular shape, which is identified in the study area map to the exact area. All sub-maps contain the city name and alternating scale bar for the miles plot. The north arrow selector is at the top of the map. The details of the cities are given in Table 3. Gathering spatiotemporal data that is pertinent to one's research question is an essential step in conducting a comprehensive and rigorous study see Fig. 1.

3.2 Exploratory Data Analysis (EDA)

The EDA of the data is divided into two parts: graphical exploratory analysis and statistical exploratory analysis. In GEA, the plots of the decomposed series are along with the autocorrelation functions ACF and PACF. The second part contains the SEA, in which a table presents the statistical summary of the air pollution $PM_{2.5}$ dataset of the US Embassy.

3.2.1 Graphical Exploratory Analysis (GEA)

The line plots see Fig. 2. depict various components and analyses of $PM_{2.5}$ values across different stations. The actual $PM_{2.5}$ values represent the observed pollution levels, while the trend component illustrates the underlying long-term patterns or trends in the data. Seasonal components highlight periodic fluctuations, potentially reflecting seasonal variations in pollution levels. The residual component captures the differences between observed and predicted values, indicating any remaining irregularities or noise in the data. The trend shows that the initial index term for all stations is almost upward trending. It is evident that the trend of the dataset is consistently fluctuating. The regular seasonal repetition pattern spans over 24 periods. The ACF and PACF plots, which revealed insights into the complex data patterns, were instrumental in this discovery. The residuals, depicting the random fluctuation of the data

Table 3 Statistical summary of air pollution $PM_{2.5}$ dataset of US Embassy station

Metric	Beijing	Chennai	Delhi	Dhaka	Islamabad	Karachi	Kolkata	Lahore	Mumbai	Peshawar	Shanghai
Latitude(°N)	39.954906	13.06041	28.59802	23.796848	33.724203	24.842301	22.546877	31.5602	19.06533	34.025917	31.208723
Longitude(°E)	116.467945	80.24963	77.1866	90.421973	73.118033	67.007855	88.351482	74.3362	72.86842	71.560135	121.447804
Altitude(m)	30–40	6–60	214–218	9–32	457–507	2.5–8	6.4–9	150–217	10–15	345–358	3-5
Count	3251	32,517	32,517	32,517	32,517	32,517	3251	32,517	32,517	32,517	32,517
Mean	35.9609	25.4245	82.7952	82.1043	41.5994	36.570	60.5432	95.964	42.6667	66.6632	27.4943
Std	33.1209	14.6626	64.1904	60.4317	23.3728	20.2700	53.2651	69.3282	33.647	37.9860	17.0419
Min	0.1	0.1	0.6	0.2	0.1	0.1	0.1	1.0	0.1	0.5	0.1
25%	12.4	15.1	34.7	34.4	25.3	23.4	19.8	47.1	14.9	39.7	15.3
50%	26.8	23.1	61.9	60.7	35.9	30.0	44.3	71.4	30.9	56.5	23.1
75%	47.3	32.2	113.8	118.9	52.6	43.5	87.7	127.6	65.9	85.5	34.6
Max	198.6	71.4	284.2	256.3	115.3	105.3	220.7	317.5	157.3	185.5	96.9

after removing trend and seasonal components, highlight the intricate nature of our data. The ACF plot of Beijing and Shanghai has no wave formation. In the PACF, strong seasonal characteristics were observed for lag1 and lag2 values.

3.2.2 Statistical Exploratory Analysis (SEA)

The dataset presented in Table 3 offers insights into the spatial distribution and features of air quality monitoring stations established by US embassies and consulates in various vital urban centers in Asia. Each station is denoted by a specific dataset code name and details regarding the city's name, geographic coordinates (latitude and longitude), and elevation above mean sea level. The towns covered encompass Beijing, Chennai, Delhi, Dhaka, Islamabad, Karachi, Kolkata, Lahore, Mumbai, Peshawar, and Shanghai. Elevation levels vary from 2.5–8 m above MSL in Karachi to 457–507 m in Islamabad, underscoring the diverse topographical conditions of these monitoring sites across South and East Asia. The dataset holds potential for examining spatial trends in $PM_{2.5}$ air pollution concentrations and their association with factors like topography, altitude, and urban development in these major metropolitan areas. Subsequently, the table delivers a detailed statistical overview of the US embassy-operated stations in major cities like Beijing, Chennai, Delhi, Dhaka, Islamabad, Karachi, Kolkata, Lahore, Mumbai, Peshawar, and Shanghai.

The Table 3 outlines various statistical parameters for each site, including frequency, average, standard deviation, minimum, 25th percentile, median, 75th percentile, and maximum values. It offers valuable insights into the distinctive attributes of each location. Delhi and Lahore record the highest average values, whereas Chennai and Shanghai exhibit the lowest levels. The wide range between the minimum and maximum values indicates a broad spectrum of data points for each site. Analysis of the statistical data from the US embassy stations highlights significant variations across the different locations. Particularly, the Lahore station stands out with the highest average of 95.964, standard deviation of 69.328, and extreme values, including the highest minimum of 1.0, 25th percentile of 47.1, median of 71.4, 75th percentile of 127.6, and maximum of 317.5. Conversely, the stations in Chennai and Shanghai demonstrate lower overall activity levels, with mean values of 25.4245 and 27.4943, respectively, along with comparatively modest standard deviations and extreme values. Other stations such as Delhi, Dhaka, and Peshawar also exhibit notable variations in their statistical profiles, emphasizing the diverse operational contexts of US embassies in these regions.

The selection of stations based on all positive spatial correlations with each other in showing in Fig. 3, where the correlation coefficient (α) is greater than or equal to 0.0059,

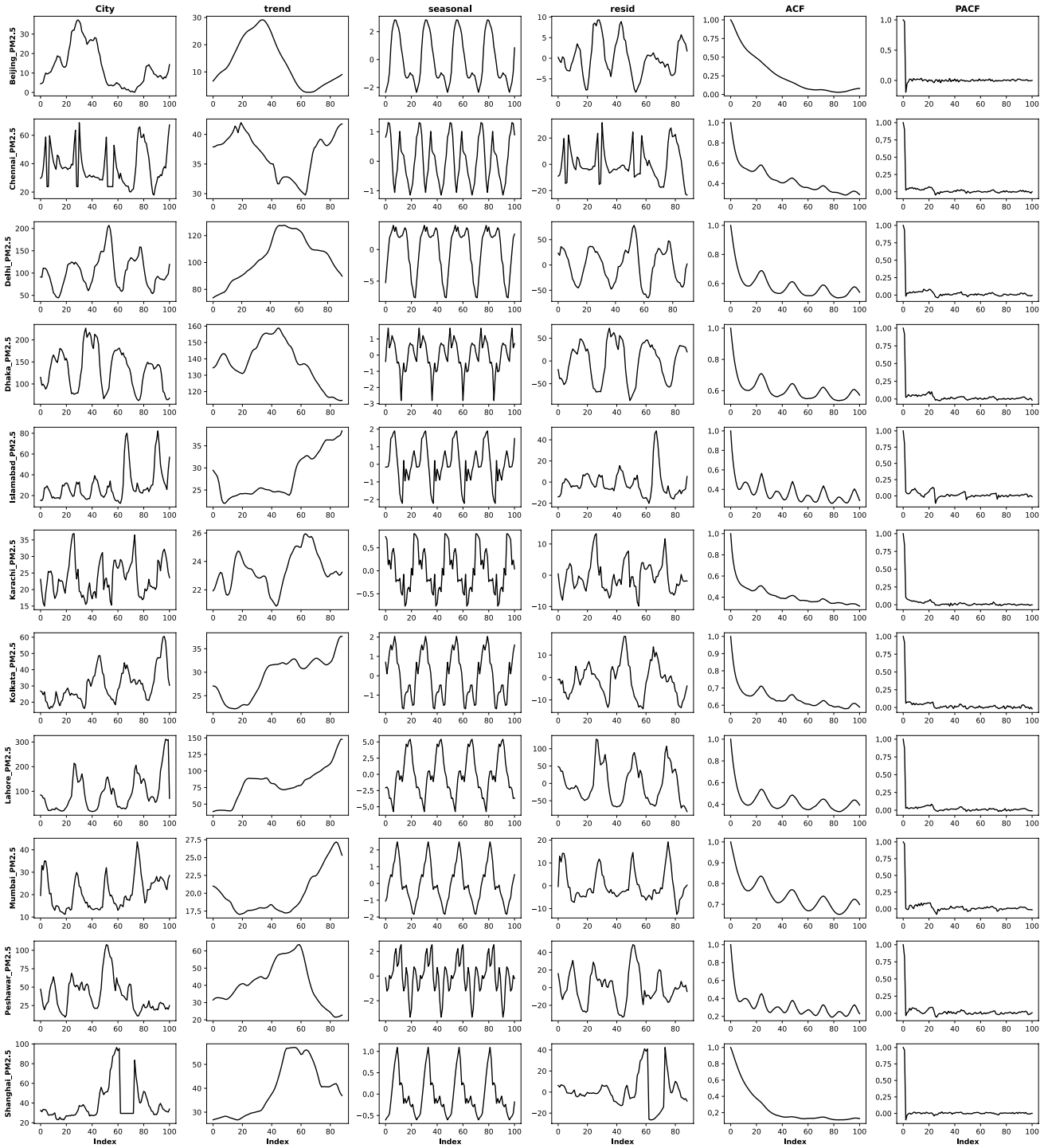

Fig. 2 The plots of decomposed series (i.e., trend, seasonal, and residual) along with autocorrelation function ACF and PACF plot

suggests a robust spatial relationship among these stations in terms of the measured parameter or variable. This criterion indicates that the stations exhibit similar trends or patterns in their respective data, implying potential spatial coherence in the observed phenomenon. By considering stations with positive spatial correlations above the specified threshold, prioritize those locations that exhibit consistent behavior or share common underlying factors influencing the variable of interest. Analyze the Spearman correlation plot see Fig. 3 to the visualization of the heat map. This analysis includes $PM_{2.5}$ concentrations from various US Embassy locations. The heatmap displays the pairwise Pearson correlation coefficients, highlighting the interdependencies within the data. This insight is crucial for understanding station relationships

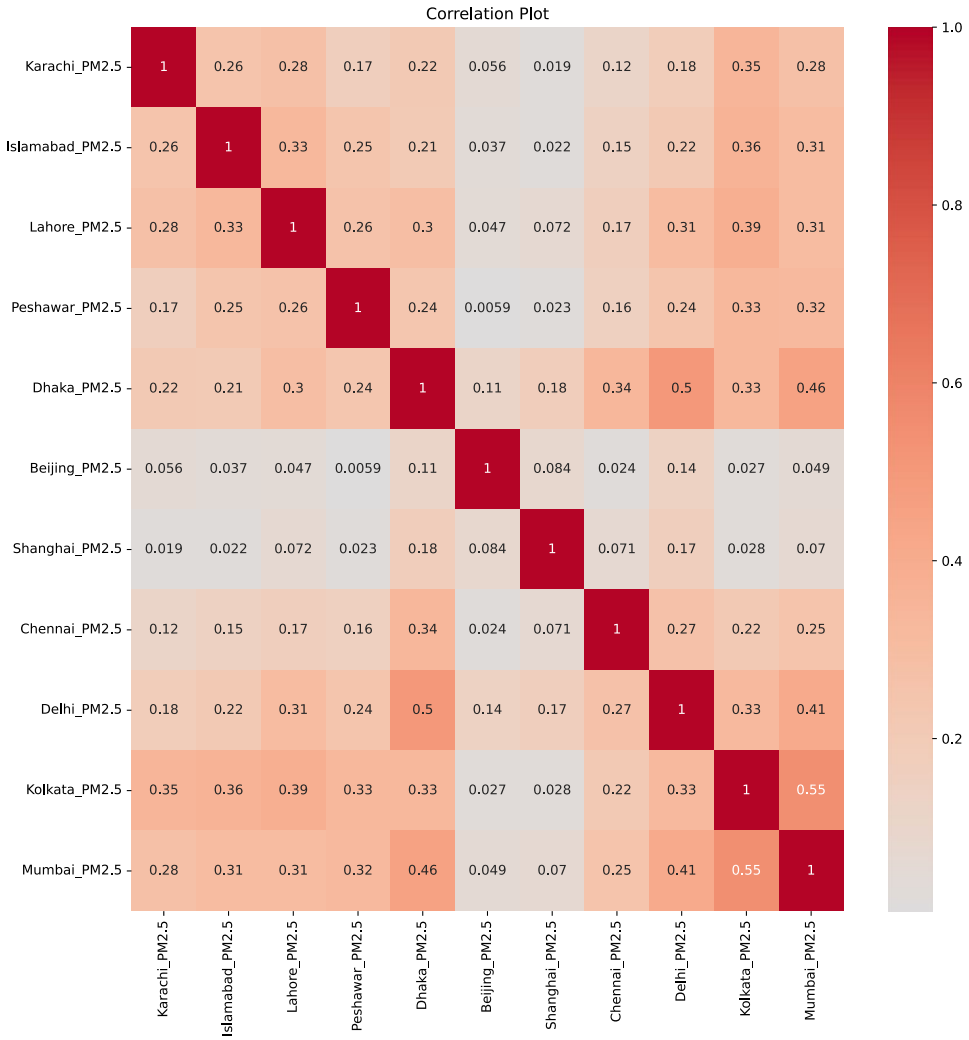

Fig. 3 The US embassies and consulate stations based on correlation to each other where $\alpha \geq 0.0059$

and selecting relevant inputs for modeling. The heat map graphically displays the correlation of the features to each other. All the selected stations positively correlate to each of the different features. These are some of the productive steps in building robust air pollution modeling. The correction heat map expresses the coherent spatial patterns of the dataset to be prepared for using the air pollution model. The autocorrelation ρ_i measures the strength and direction of the linear dependence between the time series variable x_t and its lagged value x_{t-j}. The autocorrelation ρ_i is calculated as $\rho_i = Cov(x_t, x_{t-j})/sqrt(Var(x_t) * Var(x_{t-j}))$. Here, $\mathrm{Cov}(x_t, x_{t-j})$ represents the j^{th} order autocovariance, which quantifies the direction of linear dependence between x_t and x_{t-j}. The coefficient ρ_j can identify seasonal (Se) and trend (Tre) patterns in the time series. The ρ_j values are computed for different lag values, denoted as $\mathcal{L}$ = 1, 2, 3,..., k. If at least one ρ_j value is more significant than 0.05 for all lags $\mathcal{L}$ = 1, 2, 3,..., k, it indicates the presence of a pattern in the time series. In other words, the autocorrelation coefficient ρ_j measures the linear relationship between the current value of the time series and its past values at different lags. If the autocorrelation is significant for one or more lags, it suggests the existence of a seasonal or trend pattern in the time series data.

See the proposed Algorithms 1 and 2 for a concise description.

In Table 4 summary, the results of both the ADF and KPSS tests consistently show that the time series data for all the cities are stationary. By using both tests, we cross-validate our stationarity assumption from two statistical perspectives: if ADF suggests stationarity and KPSS does not reject it, the data is considered strongly stationary. This ensures that temporal dependencies are well captured by the model without violating time-series assumptions. The stationarity of the time series is an essential assumption for many time series analysis techniques, such as regression modeling and forecasting. The results of this analysis suggest that the time series data can be used for further study and modeling without the need to perform additional transformations to achieve stationarity.

Table 4 Stationarity test using ADF and KPSS method of pollution datasets

STATION	ADF[1]						KPSS[2]					
	ADF Statistic	p-value	1 %	5 %	10%	Stationary	KPSS Statistic	p-value	1 %	5 %	10%	Stationary
Beijing	− 18.82610	2.02e− 30	− 3.430	− 2.861	− 2.566	Yes	0.67226	0.0160	0.739	0.463	0.347	Yes
Chennai	− 11.44128	6.16e− 21	− 3.430	− 2.861	− 2.566	Yes	2.70703	0.01	0.739	0.463	0.347	Yes
Delhi	− 8.30006	4.04e− 13	− 3.430	− 2.861	− 2.566	Yes	1.32523	0.01	0.739	0.463	0.347	Yes
Dhaka	− 7.16023	2.98e− 10	− 3.430	− 2.861	− 2.566	Yes	2.20745	0.01	0.739	0.463	0.347	Yes
Islamabad	− 10.30727	3.25e− 18	− 3.430	− 2.861	− 2.566	Yes	0.52159	0.036	0.739	0.463	0.347	Yes
Karachi	− 10.63276	5.16e− 19	− 3.430	− 2.861	− 2.566	Yes	0.63843	0.019	0.739	0.463	0.347	Yes
Kolkata	− 6.74010	3.13e− 9	− 3.430	− 2.861	− 2.566	Yes	1.17043	0.01	0.739	0.463	0.347	Yes
Lahore	− 9.10589	3.50e− 15	− 3.430	− 2.861	− 2.566	Yes	0.60213	0.022	0.739	0.463	0.347	Yes
Mumbai	− 7.17196	2.78e− 10	− 3.430	− 2.861	− 2.566	Yes	0.99834	0.01	0.739	0.463	0.347	Yes
Peshawar	− 11.38067	8.52e− 21	− 3.430	− 2.861	− 2.566	Yes	1.01322	0.01	0.739	0.463	0.347	Yes
Shanghai	− 17.65526	3.70e− 30	− 3.430	− 2.861	− 2.566	Yes	0.97543	0.01	0.739	0.463	0.347	Yes

Both ADF and KPSS test results suggest that the pollution datasets from all listed stations are stationary

[1] ADF: All stations have very low p-values (close to zero), which are well below the typical significance levels of 1%, 5%, and 10%. This indicates strong evidence against the null hypothesis of a unit root

[2] KPSS: The KPSS statistics for most stations are below the critical values at the 1%, 5%, and 10% levels, indicating that fail to reject the null hypothesis of stationarity for these stations

4 Deep Learning Models

Deep learning models are utilized for research. 1DCNN, GRU, RNN, and LSTM state-of-the-art models are used to compare with the proposed model. Each model has different characteristics that can be used to predict the dataset.

4.1 1-D Convolutional Neural Network (1DCNN)

A CNN is categorized as a form of supervised deep learning algorithm that proves to be exceedingly advantageous in the identification of intricate patterns within temporal dimensions while also dynamically acquiring knowledge about spatial hierarchies of characteristics via the utilization of convolution operations (Sahoo et al. 2020), pooling layers, and non-linear activation functions (Samal et al. 2021). The CNN model is frequently applied in various domains, such as predicting air pollution levels or examining data in biomedical research, computer vision, and sensor-generated data.

Let us consider a multivariate time series $\mathrm{x} = \{x_1, x_2, \ldots, x_T\}$, where each $x_t \in \mathbb{R}^F$ represents a feature vector of $\mathrm{PM}_{2.5}$ concentrations from $F = 11$ embassy stations at time step t. The convolutional operation for the 1D CNN layer can be written as:

$$y^{(l)} = \sigma\left(W^{(l)} \bigoplus X^{(l-1)} + b^{(l)}\right) \tag{1}$$

where σ is the activation function (i.e., ReLU), W^l is the weight with kernel size k for the 'c' no. of the input channel. The bias vector is denoted as b^l in $\mathbb{R}^c$, and $\bigoplus$ denotes the convolutional operation in CNN.

The pooling operation $\mathcal{P}$ can be performed as

$$z^l = \mathcal{P}(y^l) \tag{2}$$

4.2 Bidirectional-Gated Reccurent Unit (BiGRU)

The GRU, a simplified version of the RNN, incorporates gating mechanisms with a reduced parameter count compared to its precursor (Sun et al. 2023). This specific attribute significantly boosts its ability to grasp sequential patterns, resulting in learning outcomes and improved ones. The enhanced performance reinforces the efficiency and effectiveness of the GRU (Shewalkar et al. 2019). This specific feature substantially enhances its capacity to comprehend sequential patterns more effectively, improving learning outcomes. The BiGRU is designed to process input sequences by moving in both forward and backward directions concurrently (Duan et al. 2021). This advanced model

assimilates information from preceding and subsequent contexts, enhancing its overall comprehension and analysis of the provided dataset.

The advanced RNN architecture with forward and backward directions for processing sequence data is known as forward GRU and backward GRU. Each cell contains the update gate (z) and rest gate (r). Update gate (z) processes the decision to add new information and forget the previous (past) information. For each timestamp t, the forgetting of part information is decided by the reset gate (r).

The forward GRU:

$$\mathrm{fGRU}(x_t, h^f_{(t-1)}) = h^f_t = \begin{cases} z^f_t = \sigma\left(W^f_z\left[h^f_{(t-1)}, x_t\right] + b^f_z\right), \\ r^f_t = \sigma\left(W^f_r\left[h^f_{(t-1)}, x_t\right] + b^f_r\right), \\ \bar{h}^f_t = \tanh\left(W^f\left[r^f_t \otimes h^f_{(t-1)}, x_t\right] + b^f\right), \\ h^f_t = \left(1 - z^f_t\right) \otimes h^f_{(t-1)} + z^f_t \otimes \bar{h}^f_t, \end{cases} \tag{3}$$

Backward GRU:

$$\mathrm{bGRU}\left(z_t + h^b_{t-1}\right) = h^b_t = \begin{cases} z^b_t = \sigma\left(W^b_z\left[h^b_{(t-1)}, x_t\right] + b^b_z\right), \\ r^b_t = \sigma\left(W^b_r\left[h^b_{(t-1)}, x_t\right] + b^b_r\right), \\ \bar{h}^b_t = \tanh\left(W^b\left[r^b_t \otimes h^b_{(t-1)}, x_t\right] + b^b\right), \\ h^b_t = \left(1 - z^b_t\right) \otimes h^b_{(t-1)} + z^b_t \otimes \bar{h}^b_t, \end{cases} \tag{4}$$

where σ is the sigmoid activation function, W and b represent the weight and bias vector. z_t, h_t, and r_t are the update gate, hidden state, and reset gate, respectively, where $\otimes$ denotes the element-wise multiplication.

The forward h^f_t and backward hidden h^b_t state combinedly donoted as h_t

$$h_t = [h^f_t; h^b_t] \tag{5}$$

Now the output layer can obtain the forecasted value $\hat{y}_t$ i.e., denoted as shown in eqn below:

$$\hat{y}_t = (W_o h_t + b_o) \tag{6}$$

where b_o and W_o are the bias vectors and output weight.

5 Methodology

Let's consider the vector X=$\{ x_1, x_2,....,x_n\} = \{ x_i\}^n_{i=1}$, here each x_i represents a random variable in the time series, indexed by time step *t*, capturing the temporal dynamics of the $PM_{2.5}$ concentrations. The raw $PM_{2.5}$ data at each station is a 1D time series, but when combining data from multiple embassy stations, the final input becomes a 2D multivariate time-series matrix. This vector captures a time series of n random variables over time. Missing data imputation is one of the hectic tasks in preprocessing the data. After completing the same, the mean of the observed column values was imputed into the missing place.

$\hat{x}_{ij} = \begin{cases} x_{ij}, & \text{if } x_{ij} \text{ is observed} \\ \bar{x}_j, & \text{if } x_{ij} \text{ is missing} \end{cases}$, Let x_{ij} denote the observed (actual) data in the dataset's i^{th} row and j^{th} column, where i = 1, 2,..., m represents the rows, and j = 1, 2,..., n represents the columns. Imputation of missing values $\hat{x}_{ij}$ in each column j using the respective column mean $\bar{x}_j$: where $\bar{x}_j = \frac{1}{m}\sum_{i=1}^{m} x_{ij}$.

5.1 Proposed 1: Hybrid 1d-Convolutional Neural Network and Bidirectional Gated Recurrent Unit (1DCNN-BiGRU) Model

The 1DCNN component performs feature extraction by convolving over the input data, extracting relevant spatial features to capture local patterns. The Bidirectional GRU layer enhances the model's ability to capture long-range dependencies and temporal dynamics by simultaneously processing input sequences in forward and backward directions. This bidirectional processing allows the model to leverage context from past and future timestamps, enabling a more comprehensive understanding and prediction of sequential data Fig. 4. See the proposed algorithms 1 and 2 for a concise description.

For each convolutional layer (l), the 1DCNN method has a convolutional operation followed by a max pooling operation, which can be written as given below:

$$y^l = \sigma(W^l \cdot X^{t-1} + b^l) \tag{7}$$

$$z^l = \mathcal{P}(y^l) \tag{8}$$

then the final output of CNN can be obtained as Z^L = [z_1, z_2,....,z_m] i.e., Z $\in \mathbb{R}^c$ for last CNN layer. The reshape of 1DCNN output i.e., Z^L can be done as:

$$c = Reshape(Z^L) \tag{9}$$

where c =$\{ c_1, c_2,....,c_n\}$ and $c_i \in \mathbb{R}^n$,

Now, the component of BiGRU for each time step (t= 1, 2, 3,.....n) for forward GRU and backward GRU obtained and combined both, can be written as Equ. 5

$$h_t = \begin{cases} h^f_t = \mathrm{fGRU}\left(z_t, h^f_{(t-1)}\right) \\ h^b_t = \mathrm{bGRU}\left(z_t, h^b_{(t-1)}\right) \end{cases} \tag{10}$$

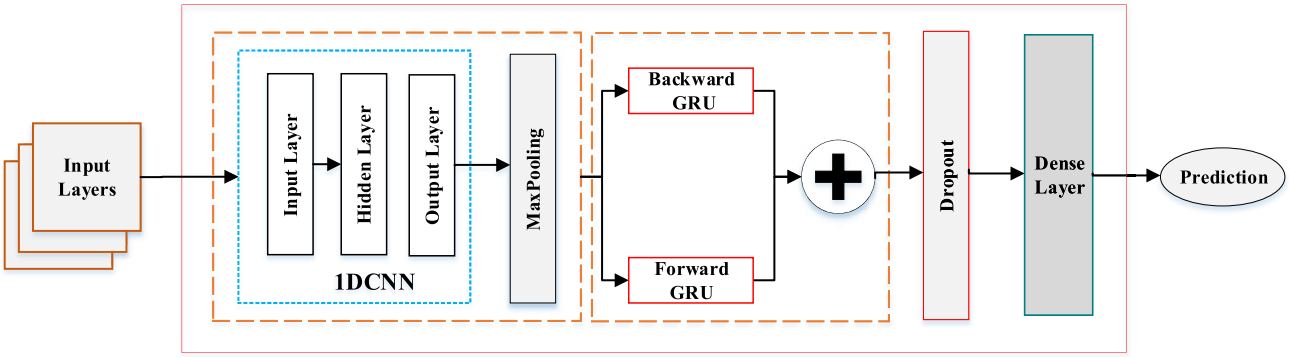

Fig. 4 The proposed-1 (1DCNN-Bidirectional GRU) hybrid network model architecture

Now, the forecasted value $\hat{y}$ of hybrid 1DCNN-BiGRU can be obtained

$$\hat{y}_t = (W_0 h_t + b_0) \tag{11}$$

where h_t denotes the hidden state at the last timestep T. W_0 and b_0 indicate the weight matrix and bias vectors at the output layer.

Now, firstly, the decomposition of the data sequence (X) additive decomposition can be obtained in seasonal (X_{Se}), trend (X_{Tre}), and residual (X_{Re}). Lets consider $X_i \in \{X_{Se}, X_{Tre}, X_{Re}\}$ is the decomposed series. Then, for each X_i decomposed series, a data sequence can be denoted as $X_i = \{X_{i,1}, X_{i,2}, X_{i,3}, \ldots\ldots X_{i,t}\}$ where i ∈ {Se, Tre, Re} and $x_{i,j} \in \mathbb{R}^f$. Then, the convolutional layer of 1DCNN can be denoted as:

Input: Feature set $X = \{x_1, x_2, \ldots, x_n\}$ *(Uni-variate US embassies $PM_{2.5}$ dataset)*
Output: $\hat{y}_t$ *(Final prediction of proposed model)*

1. Initialization: The vector captures a time series of n random variables.
2. 1DCNN training: $y^l = \sigma(W^l \cdot X^{t-1} + b^l)$ *(see Equation 1)*
3. Pooling operation: $z^l = \mathcal{P}(y^l)$
4. The output of max-pooling is the input for BiGRU:
   The input gate of BiGRU will utilize the forward direction followed by the backward direction as:
   (a) Forward: $h_t^f = \text{fGRU}(z_t, h_{(t-1)}^f)$ *(see Equation 3)*
   (b) Backward: $h_t^b = \text{bGRU}(z_t, h_{(t-1)}^b)$ *(see Equation 4)*
5. Combine forward h_t^f and backward h_t^b for the output of BiGRU: $h_t = [h_t^f; h_t^b]$ *(see Equation 5)*
6. For the final prediction: $\hat{y}_t = W_0 h_t + b_0$

Return: $\hat{y}_t$

Algorithm 1 Proposed-1: 1DCNN-BiGRU model for $PM_{2.5}$ pollutant prediction

5.2 Proposed 2: Hybrid 1d-Convolutional Neural Network and Bidirectional Gated Recurrent Unit with Decompose-Recompose (1DCNN-BiGRU-DR) model

The proposed-1 model demonstrates the input data X process by 1DCNN to extract the information Z, which is the input for the BiGRU to capture the temporal dependencies. Finally, the last hidden layer produces the prediction $\hat{y}$. Lets consider a model $H_m(X)$ denotes the 1DCNN-BiGRU hybrid model which takes the training input and predict $\hat{y}$ as:

$$\hat{y} = H_m(X) \tag{12}$$

$$\left.\begin{aligned} y_i^l &= \sigma\left(w_i^l \times x_i^{(l-1)} + b_i^l\right) \\ z_i^l &= \mathcal{P}\left(y_i^l\right) \end{aligned}\right\} \tag{13}$$

which produces the final CNN output:

$$Z_i = [Z_{i,1}, Z_{i,2}, Z_{i,3}, \ldots\ldots Z_{i,m}) \tag{14}$$

where $Z_{i,j} \in \mathbb{R}^c$ and Z_i represents the CNN output component. The output Z_i is processed for time-step t with the following steps:

$$\left.\begin{aligned} h_{i,t}^{f} &= \text{fGRU}\left(z_{i,t}, h_{i,g}^{f}(t-1)\right) \\ h_{i,t}^{b} &= \text{bGRU}\left(z_{i,t}^{b}, h_{i,o}^{b}(t+1)\right) \\ h_{i,t} &= \left[h_{i,t}^{f}, h_{i,t}^{b}\right] \end{aligned}\right\} \tag{15}$$

So, the output layer of BiGRU has $\hat{y}$ i.e., denoted as (see Equ. 7):

$$\hat{y}_i = W_{o,i} * h_{i,T} + b_{o,i} \tag{16}$$

Now, for each i ∈ {Se, Tre, Re}, the forecasting of $H_m(X_{Se})$, $H_m(X_{Tre})$, and $H_m(X_{Re})$ can be obtained as $\hat{y}_{Se}$, $\hat{y}_{Tre}$, and $\hat{y}_{Re}$. So, the aggregation (Recompose) of $\hat{y}_{Se}$, $\hat{y}_{Tre}$, and $\hat{y}_{Re}$ can be performed to obtain $\hat{Y}_{DR}$ final prediction that can be denoted as:

$$\hat{Y}_{DR} = \hat{y}_{Se} + \hat{y}_{Tre} + \hat{y}_{Re} \tag{17}$$

The $\hat{Y}_{DR}$ prediction captures the different aspects of the time series separately before combining them into the final forecast. The proposed 1DCNN-BiGRU decomposed-recomposed approach utilizes the propose-1 hybrid model to learn through the seasonal, trend, and residual characteristics, which enable enhanced performance.

Splitting the data into the train 70%, validation 15%, and test 15%. After splitting the dataset, decomposed the dataset into three specific formats: resid, seasonal, and trend. In model selection, authors have utilized the proposed-1 model with hand-tuning parameters. After model selection, all resid, seasonal, and trend predictions were recomposed. Finally, performance measures are evaluated using unseen test data.

6.1 Parameters Setting of Deep Learning Models

The Table 5 compares traditional and proposed-1 model configurations. Each model's distinctive layer setup and parameters are outlined, offering insights into its architecture and optimization choices. For all models, a window length of 8, a batch size ranging from 8 to 200, and 11 features are used, with training epochs set to 200. Additionally, strategies such as ReduceLROnPlateau, with parameters monitoring validation loss, patience of 3 epochs, and a reduction factor of 0.5, coupled with a cooldown of 1 epoch, as well as EarlyStopping monitoring validation loss with a patience of 15 epochs and restoring the best weights, are employed. For instance, the 1DCNN model incorporates a

Input: Feature set $X = \{x_1, x_2, ..., x_n\}$ *(Uni-variate US embassies $PM_{2.5}$ dataset)*
Output: $\hat{Y}_{DR}$ *(Final prediction of proposed model)*

1. Initialization: 1DCNN-BiGRU Hybrid model which takes the training input and predicts $\hat{y}$.
2. **Apply the following steps for component i with the utilization of proposed-1 model:**
   (a) 1DCNN training: $y_i^l = \sigma\left(w_i^l \times x_i^{(l-1)} + b_i^l\right)$ *(see Equation 13)*
   (b) Pooling operation: $z_i^l = P\left(y_i^l\right)$
   (c) Input to BiGRU:
      (i) Forward: $h_{i,t}^f = \text{fGRU}\left(z_{i,t}, h_{i,g}^f(t-1)\right)$ *(see Equations 15)*
      (ii) Backward: $h_{i,t}^b = \text{bGRU}\left(z_{i,t}, h_{i_0(t+1)}^b\right)$
   (d) Combine forward and backward outputs: $h_{i,t} = \left[h_{i,t}^f, h_{i,t}^b\right]$
3. **Recompose the predictions from each component:** *(see Equations 16 and 17)*
   (a) For each $i \in \{Se, Tre, Re\}$:
   (b) $\hat{y}_i = W_{o,i} h_{i,T} + b_{o,i}$
4. The final prediction will be measured with method $\hat{Y}_{DR} = \hat{Y}_{Se} + \hat{Y}_{Tre} + \hat{Y}_{Re}$

Return: $\hat{Y}_{DR}$

Algorithm 2 Proposed-2: 1DCNN-BiGRU-DR model for $PM_{2.5}$ pollutant prediction

6 Experimental Setup

The flowchart see Fig. 5 of the proposed work commences by accessing the dataset provided by the US embassies, with a specific focus on $PM_{2.5}$ levels. The flowchart deals with initial data preprocessing tasks, such as handling missing values and accounting for temporal and spatial correlations. 1D convolutional layer with 64 filters and LeakyReLU activation, followed by max pooling and a dense output layer, employing the Nadam optimizer with a specified learning rate and MSLE loss function. Conversely, the 1DCNN-GRU model combines 1DCNN and GRU layers with flexible configurations, including variable dropout rates and optimizer options such as Adam or Nadam, providing adaptability

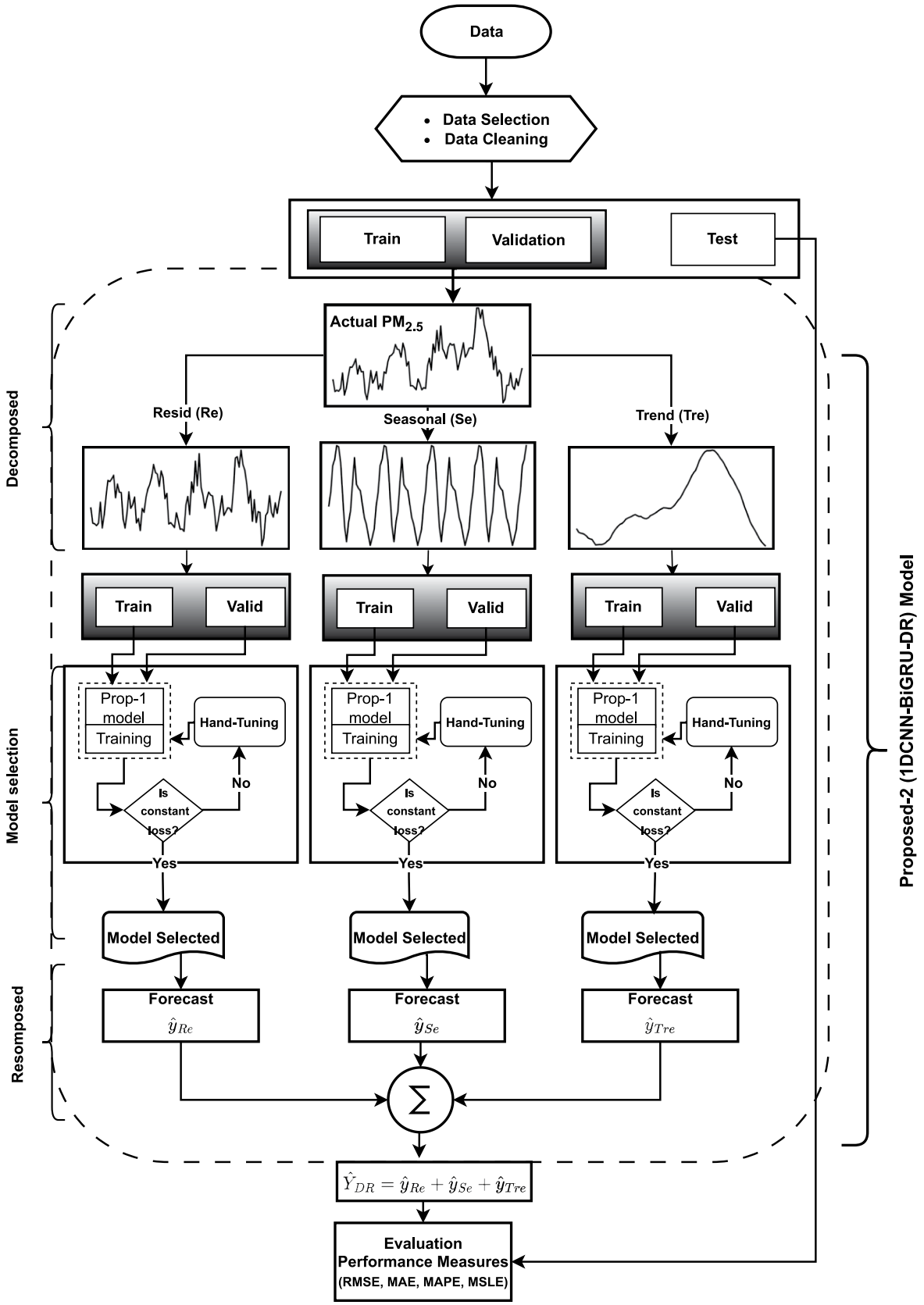

Fig. 5 The framework of proposed-2 1DCNN-BiGRU-DR modeling to the $PM_{2.5}$ forecasting

Table 5 Acchitecture layer-wise description of the traditional models and proposed models

Model	Configuration
1DCNN	Input → Conv1D (64 filters, kernel=2, input shape=(win length, num features)) → LeakyReLU → MaxPool1D(2) → Flatten() → Dense (1). Optimizer: Nadam(0.001), Loss: MSLE
LSTM	Input → LSTM (156 units, return_ sequences=True, input shape=(win length, num features)) → Flatten() → Dense (1). Optimizer: Nadam(0.001), Loss: MSLE
BiLSTM	Input → BiLSTM (128 units, return_ sequences=True, input shape=(win length, num features)) → Flatten() → Dense (1). Optimizer: Nadam(0.001), Loss: MSLE
GRU	Input → GRU (128 units, return_sequences=True, input shape=(win length, num features)) →Flatten() → Dense (1) Optimizer: Nadam(0.001), Loss: MSLE
RNN	Input → SimpleRNN (128 units, return_ sequences=True, input shape=(win length, num features)) → Flatten() → Dense (1). Optimizer: Nadam(0.001), Loss: MSLE
Proposed	Input → Conv1D (32-128 filters, kernel=3-5, dilation rate=1-2), input shape=(win length, num features) → activation= LeakyReLU, ReLU → MaxPool1D(2) → BiGRU (16-128 units, return_sequences=True, activation=LeakyReLU, ReLU) → Dropout(0.2− 0.5) → Flatten() → Dense (1) Optimizer: Adam(0.1− 0.001)-Nadam(0.1− 0.001), Loss: MSE-MSLE

for different tasks and datasets. This tabular format facilitates a quick comparison, aiding practitioners in selecting appropriate model architectures and optimization strategies based on specific requirements and constraints. The Table 6 showcases various performance metrics employed to evaluate prediction accuracy for individual stations i. The metrics included are the RMSE, MAE, MAPE, and MSLE. Each metric is defined alongside its respective formulae, equation number for reference, and a description elucidating the variables involved, such as predicted ($\hat{p}_i$) and actual (x_i) values, time steps (T), and the inclusion of a small constant c to prevent division by zero in the MAPE calculation.

6.2 Hardware and Software Required

The Table 7 provides a comprehensive overview of the computing environment. The components listed in the table include the operating system, CPU, RAM, GPU, storage, Python version, deep learning frameworks, integrated development environment, and other libraries used, along with their respective descriptions. The operating system is specified as Windows 10 Professional 64-bit, and the CPU is identified as an Intel Core i5-9500 CPU running at 3.00GHz with six cores and six logical processors. The system has 16 GB of DDR4 RAM and an Intel UHD Graphics 630 GPU with 8 GB of shared memory. A 1 TB HDD provides storage capacity. The software environment encompasses Python 3.9.12 from the Anaconda Distribution and deep learning frameworks PyTorch 1.10.2 and TensorFlow 2.10.0. Development and coding are facilitated by Visual Studio Code 1.60.2 and Jupyter Notebook 6.4.12. Additionally, the environment incorporates essential libraries such as NumPy 1.24.3, Pandas 1.4.3, Matplotlib 3.7.1, and Scikit-learn 1.1.1. This table summarizes the computing setup utilized for various tasks and projects.

7 Results and Analysis

The proposed models across 11 US embassies selected stations use four key metrics, RMSE, MAE, MAPE, and MSLE, to assess predictive accuracy and model quality. It is generally accepted that the model with the lowest accuracy metric values is considered the "best" among competing models. The spanning of the testing data from October 4, 2022, at 17:00 to August 6, 2023, at 23:00, this Tables 8, 9, and 10 offers a detailed evaluation of the model's performance in forecasting $PM_{2.5}$ concentration.

Table 6 Performance metrics for predicting accuracy are used for quantitative evaluation

Metric	Formula	Variable Description
Root Mean Squared Error (RMSE)	$\mathrm{RMSE}_i = \sqrt{\frac{1}{T}\sum_{t=1}^{T}(\hat{p}_i[t] - x_i[t])^2}$	Predicted ($\hat{p}_i$) and actual (x_i) values for each station i, T is the number of time steps
Mean Absolute Error (MAE)	$\mathrm{MAE}_i = \frac{1}{T}\sum_{t=1}^{T}\lvert\hat{p}_i[t] - x_i[t]\rvert$	Predicted ($\hat{p}_i$) and actual (x_i) values for each station i, T is the number of time steps
Mean Absolute Percentage Error (MAPE)	$\mathrm{MAPE}_i = \frac{1}{T}\sum_{t=1}^{T}\left\lvert\frac{\hat{p}_i[t]-x_i[t]}{x_i[t]+c}\right\rvert \times 100\%$	Predicted ($\hat{p}_i$) and actual (x_i) values for each station i, T is the number of time steps, c is a small constant
Mean Squared Logarithmic Error (MSLE)	$\mathrm{MSLE} = \frac{1}{n}\sum_{i=1}^{n}(\log(p_i+1) - \log(x_i+1))^2$	Predicted (p_i) and actual (x_i) values for each station i, n is the total number of samples

Table 7 The list of the computing environment, i.e., hardware and software

S. no.	Component	Description
1	Operating System	Windows 10 Professional (64-bit)
2	CPU	Intel Core i5-9500 CPU @ 3.00GHz (6 cores, 6 logical processors)
3	RAM	16 GB DDR4
4	GPU	Intel(R) UHD Graphics 630 (8 GB Shared GPU memory)
5	Storage	1 TB HDD
6	Python Version	Python 3.9.12 (Anaconda Distribution)
7	Deep Learning Framework	PyTorch 1.10.2, TensorFlow 2.10.0
8	IDE	Visual Studio Code 1.60.2, Jupyter Notebook 6.4.12
9	Other Libraries	NumPy 1.24.3, Pandas 1.4.3, Matplotlib 3.7.1, Scikit-learn 1.1.1

7.1 Quantitative Analysis

In this section of the quantitative analysis, the performance measures (RMSE, MAE, MAPE, and MSLE) are compared to prop-1 with traditional deep learning, prop-2 with traditional deep learning, and prop-2 with DL-DR deep learning models on the test datasets of the US Embassy.

7.1.1 Proposed-1 (1DCNN-BiGRU) Hybrid Model Versus Traditional Deep Learning Model

The Table 8 compares the performance of different models, including CNN, BiLSTM, GRU, LSTM, RNN, and the prop-1 model. The models were evaluated across different locations, and their performance was measured using various error metrics. The performance of the prop-1 model is highlighted in bold for each station and error metric, and the optimal values achieved are also emphasized.

- **RMSE**: The prop-1 model has a minimum of RMSE 4.26 in Shanghai and a maximum of RMSE 38.31 in Lahore compared to all traditional DL overall embassies. The maximum percentage improvement to CNN-Delhi was 392 %, and the minimum percentage improvement to BiLSTM-Chennai was 4.66%. For example, at the station Beijing, the RMSE values for the prop-1 model range from 6.92 to 12.673, showcasing its superiority over other models. In some cases, the improvement is substantial. For instance, at station Peshawar, the RMSE value for the prop-1 is 21.96, representing a significant improvement over other models, with percentage improvements ranging from 59.12% to 107.22%. The prop-1 model consistently outperforms other models across most stations regarding RMSE. Lower RMSE values indicate better model performance.
- **MAE**: The prop-1 model minimum MAE is 2.27 in Shanghai, and the maximum MAE is 19.62 in Lahore compared to all traditional DL overall embassies. The maximum percentage improvement to CNN-Delhi was 819.93 %, and the minimum percentage improvement to CNN-Chennai was 15.92%. The prop-1 model generally achieves lower MAE values than others, indicating better accuracy in predicting the target variable.
- **MAPE**: The prop-1 model minimum MAPE 10.52 in Shanghai and maximum MAPE 88.09 in Beijing compared to all traditional DL overall embassies. The maximum improvement to RNN-Delhi was 982.06 %, and the minimum improvement to RNN-Chennai was − 7.70% with MAPE 81.30. Stations like Delhi and Peshawar significantly improve MAPE with the prop-1 model. The prop-1 model showcases competitive performance in MAPE, often achieving lower percentage errors than other models.
- **MSLE**: The prop-1 model minimum MSLE 0.0204 got Shanghai and maximum MSLE 0.1471 RNN-Beijing compared to all traditional DL overall embassies. The maximum percentage improvement to CNN-Delhi was 39753.02 %, and the minimum percentage improvement to RNN-Chennai was 9.58%. There are exceptions where the improvement is less pronounced, such as in stations like Karachi and Lahore. Once again, the prop-1 model demonstrates superior performance across many stations, as indicated by lower MSLE values.

The prop-1 model outshines traditional deep learning models in terms of consistent improvement percentages across various metrics and stations. The prop-1 model performs competitively or even better than the conventional models, proving its effectiveness in modeling the dataset. The rate of improvement varies by station and error metric, but the prop-1 model consistently demonstrates superior performance. The prop-1 model has the potential to be a game-changer in the field of forecasting and analysis. Its results highlight the benefits of using it in practical applications.

7.1.2 Proposed-2 (1DCNN-BiGRU-DR) Model Versus Traditional Deep Learning

The Table 9 appears to present the performance measures of the prop-2 model compared to traditional deep learning models, including CNN, BiLSTM, GRU, LSTM, and RNN, across various US embassies' datasets. The evaluation metrics used are RMSE, MAE, MAPE, and MSLE. For RMSE, the percentage improvement (% imp) of the Proposed-DR model over traditional models is notable across different locations

Table 8 Performance comparison of traditional and proposed-1 deep learning model using RMSE, MAE, MAPE, and MSLE of US Embassies dataset (Traditional vs. Prop-1)

Error	Station	CNN	% imp	BiLSTM	% imp	GRU	% imp	LSTM	% imp	RNN	% imp	Prop-1
RMSE	Beijing	9.23	33.32%	8.89	28.43%	9.30	34.31%	9.59	38.58%	12.673	83.01%	**6.92**
	Chennai	8.81	7.61%	8.56	4.66%	8.74	6.82%	8.876	8.41%	8.855	8.16%	**8.18**
	Delhi	127.23	392.02%	29.85	15.46%	41.88	61.96%	47.07	82.03%	73.064	182.54%	**25.85**
	Dhaka	38.34	22.73%	32.93	5.44%	39.21	25.52%	40.45	29.50%	56.169	79.81%	**31.23**
	Islamabad	18.61	8.67%	28.52	66.50%	18.48	7.88%	23.20	35.46%	20.323	18.62%	**17.13**
	Karachi	13.88	15.86%	22.40	86.97%	14.28	19.18%	22.62	88.80%	13.661	14.01%	**11.98**
	Kolkata	32.73	15.58%	30.36	7.21%	33.74	19.17%	38.99	37.68%	37.131	31.11%	**28.31**
	Lahore	50.05	29.42%	44.44	14.93%	55.82	44.33%	56.75	46.74%	56.446	45.95%	**38.67**
	Mumbai	16.54	12.94%	16.37	11.75%	18.43	25.86%	20.90	42.70 %	18.625	27.13%	**14.6**
	Peshawar	41.34	88.26%	45.18	105.72%	34.94	59.12%	45.51	107.22%	38.752	76.44%	**21.96**
	Shanghai	5.64	32.36%	4.94	15.83%	5.72	34.15%	5.99	40.40%	6.50	52.35%	**4.26**
	STD	33.0432		13.230		15.644		16.654		21.621		**10.579**
MAE	Beijing	5.09	74.78%	5.07	74.14%	5.1	77.12%	5.35	83.66%	6.00	105.93%	**2.91**
	Chennai	4.92	15.92%	5.03	18.39%	5.049	18.80%	5.23	23.07%	5.23	23.08%	**4.25**
	Delhi	103.65	819.93%	16.05	42.44%	28.7	154.71%	33.72	199.33%	60.66	438.39%	**11.26**
	Dhaka	24.25	50.80%	18.787	16.83%	25.73	60.06%	28.01	74.21%	44.76	178.35%	**16.08**
	Islamabad	11.96	24.81%	20.06	109.32%	12.13	26.55%	17.95	87.25%	14.41	50.39%	**9.58**
	Karachi	8.09	33.43%	15.52	155.79%	8.57	41.27%	15.62	157.56%	7.96	31.33%	**6.06**
	Kolkata	18.70	31.55%	17.30	21.69%	20.24	42.37%	25.50	79.42%	22.87	60.90%	**14.21**
	Lahore	33.07	68.51%	27.98	42.61%	39.55	101.54%	40.95	108.66%	38.97	98.61%	**19.62**
	Mumbai	10.59	20.05 %	10.59	20.16%	12.56	42.43%	14.65	66.18%	11.43	29.58%	**8.82**
	Peshawar	29.59	130.41%	31.98	148.99%	26.70	107.88%	32.31	151.58%	31.47	145.01%	**12.84**
	Shanghai	3.33	46.712%	2.816	23.78%	3.3	49.16%	3.58	57.69%	3.71	63.32	**2.27**
	STD	27.306		8.872		11.332		12.160		18.157		**5.365**
MAPE	Beijing	86.50	− 1.81%	113.43	28.75%	89.56	1.66%	93.77	6.43%	**81.30**	− 7.70%	88.09
	Chennai	17.22	19.41%	17.44	20.92%	17.30	19.95%	17.87	23.88%	16.36	13.40%	**14.42**
	Delhi	101.30	598.09%	18.54	27.77%	44.06	203.63%	52.87	264.36%	157.02	982.06%	**14.51**
	Dhaka	25.61	64.64%	18.66	19.96%	27.06	73.95%	32.41	108.35%	57.06	266.8%	**15.55**
	Islamabad	24.45	37.42%	41.82	135.0%	24.56	38.00%	41.32	132.18%	30.66	72.29%	**17.79**
	Karachi	20.38	41.94%	44.67	211.08%	21.53	49.94%	44.85	212.32%	19.78	37.75%	**14.36**
	Kolkata	22.95	47.91%	19.73	27.10%	23.12	48.97%	28.81	85.61%	23.44	51.05%	**15.52**
	Lahore	33.36	91.3%	25.96	48.8%	42.81	145.4%	46.57	167.00%	38.12	118.56%	**17.44**
	Mumbai	20.77	33.08%	18.71	19.90%	26.48	69.67%	28.53	82.79%	18.64	19.43%	**15.60**
	Peshawar	42.63	151.10%	42.90	152.69%	44.63	162.87%	43.53	156.44%	62.24	266.64%	**16.97**
	Shanghai	14.51	37.85%	12.39	17.68%	14.73	39.94%	15.04	42.92%	14.44	37.22%	**10.52**
	STD	29.240		28.776		**21.204**		21.358		42.495		22.045

Table 8 (continued)

Error	Station	CNN	% imp	BiLSTM	% imp	GRU	% imp	LSTM	% imp	RNN	% imp	Prop-1
MSLE	Beijing	0.2074	41.02%	0.2448	66.41%	0.2020	37.34%	0.2117	43.93%	0.1849	25.74%	**0.1471**
	Chennai	0.0606	25.08%	0.0570	17.68%	0.0593	22.34%	0.0610	25.92%	0.0531	9.58%	**0.0484**
	Delhi	19.4204	39753.02%	0.0634	30.30%	0.1940	298.29%	0.2484	409.84%	0.8822	1710.4%	**0.0487**
	Dhaka	0.1137	78.10%	0.0745	16.64%	0.1158	81.29%	0.1377	115.6%	0.3062	379.31%	**0.0638**
	Islamabad	0.1069	32.86%	0.3118	287.62%	0.1035	28.6%	0.2041	153.7%	0.1357	68.71%	**0.0804**
	Karachi	0.07585	46.6%	0.2706	423.1%	0.0800	54.79%	0.2771	435.74%	0.0697	34.76%	**0.0517**
	Kolkata	0.10922	51.12%	0.0879	21.7%	0.1084	50.10%	0.1511	109.1%	0.1132	56.66%	**0.0722**
	Lahore	0.16273	121.70%	0.1103	50.29%	0.2149	192.91%	0.2350	220.20%	0.1933	163.4%	**0.0733**
	Mumbai	0.0705	46.64%	0.0604	25.77%	0.0968	101.39%	0.1196	148.88%	0.06541	36.02%	**0.0480**
	Peshawar	0.2853	409.82%	0.3441	515.37%	0.2225	297.62%	0.3519	528.90%	0.3217	474.88%	**0.0559**
	Shanghai	0.0348	70.69%	0.0269	32.01%	0.0352	72.24%	0.0374	83.1%	0.0340	66.67%	**0.0204**
	STD	5.8189		0.1174		0.0663		0.0942		0.2419		**0.0319**

Bold font indicate the best value(s) in row-wise comparision

- **RMSE**: In Beijing, the prop-2 model achieved an RMSE of 6.47, improving by 42.60% over CNN, 37.38% over BiLSTM, and 95.76% over RNN. Similar significant improvements are observed in other locations, such as Chennai, Delhi, and Dhaka, indicating the robustness and superior performance of the prop-2 model in reducing prediction errors compared to traditional DL models. Overall, the proposed-DR model consistently outperforms the traditional models, demonstrating its efficacy in various settings.
- **MAE**: The MAE performance of the prop-2 model against traditional deep learning models, including CNN, BiLSTM, GRU, LSTM, and RNN, across various US embassies' datasets. The MAE results reveal that the prop-2 model consistently delivers lower error rates than traditional models. For instance, in Beijing, the prop-2 model achieves an MAE of 3.46, representing a 47.09% improvement over CNN, 46.56% over BiLSTM, and 73.31% over RNN. In Delhi, the prop-2 model's MAE of 13.62 indicates significant improvements of 660.86% over CNN and 345.30% over RNN. Other cities such as Chennai, Dhaka, and Karachi exhibit marked enhancements with the prop-2 model. Despite occasional negative improvements, which indicate that the traditional models sometimes performed better, the overall trend demonstrates the superior performance of the proposed DR model in minimizing prediction errors across different geographical locations.
- **MAPE**: The MAPE performance of the prop-2 model versus traditional deep learning models, including CNN, BiLSTM, GRU, LSTM, and RNN, across various US embassies' datasets. The results illustrate that the prop-2 model generally offers substantial improvements or competitive performance in MAPE, though there are instances where traditional models perform better. For example, in Beijing, the prop-2 model achieves a MAPE of 90.6, slightly declining compared to some conventional models but still maintaining robustness. In Chennai, the prop-2 model has a MAPE of 19.13, worse than traditional models, indicating negative improvements. Conversely, in Delhi, the prop-2 model's MAPE of 18.5 represents a massive improvement of 447.58% over CNN and 748.75% over RNN. The trend continues with varied results across other cities, such as Karachi and Peshawar, where the prop-2 model either shows significant improvements or is slightly less effective than traditional models. This mixed performance in MAPE highlights the complexities and diverse challenges in different datasets and locations.
- **MSLE**: The MSLE performance of the prop-2 model versus traditional deep learning models, such as CNN, BiLSTM, GRU, LSTM, and RNN, across various US

Table 9 Performance comparison of traditional and proposed-2 deep learning model using RMSE, MAE, MAPE, and MSLE of US Embassies dataset (Traditional vs. Prop-2)

Error	Station	CNN	% imp	BiLSTM	% imp	GRU	% imp	LSTM	% imp	RNN	% imp	Prop-2
RMSE	Beijing	9.23	42.60%	8.89	37.38%	9.30	43.66%	9.60	48.23%	12.67	95.76%	**6.47**
	Chennai	8.81	10.93%	8.57	7.89%	8.75	10.12%	8.88	11.76%	8.86	11.50%	**7.94**
	Delhi	127.24	389.63%	29.86	14.90%	41.88	61.18%	47.07	81.15%	73.06	181.16%	**25.98**
	Dhaka	38.34	23.27%	32.94	5.90%	39.21	26.07%	40.45	30.06%	56.17	80.59%	**31.10**
	Islamabad	18.62	11.18%	28.53	70.35%	18.48	10.37%	23.21	38.59%	20.32	21.36%	**16.74**
	Karachi	13.88	22.19%	22.40	97.18%	14.28	25.69%	22.62	99.10%	13.66	20.23%	**11.36**
	Kolkata	32.73	20.36%	30.36	11.64%	33.75	24.10%	38.99	43.37%	37.13	36.54%	**27.19**
	Lahore	50.05	19.41%	44.45	6.04%	55.82	33.17%	56.75	35.40%	56.45	34.66%	**41.91**
	Mumbai	16.55	25.36%	16.37	24.04%	18.44	39.71%	20.91	58.40%	18.63	41.12%	**13.19**
	Peshawar	41.35	73.97%	45.18	90.12%	34.95	47.04%	45.51	91.50%	38.75	63.05%	**23.76**
	Shanghai	5.65	34.91%	4.94	18.06%	5.72	36.73%	5.99	43.10%	6.50	55.28%	**4.18**
	STD	33.044		13.231		15.644		16.652		21.620		**11.305**
MAE	Beijing	5.09	47.09%	5.07	46.56%	5.16	49.07%	5.35	54.57%	6.00	73.31%	**3.46**
	Chennai	4.93	2.16%	5.03	4.34%	5.05	4.70%	5.23	8.46%	5.23	8.47%	**4.82**
	Delhi	103.66	660.86%	16.05	17.81%	28.70	110.67%	33.73	147.57%	60.66	345.30%	**13.62**
	Dhaka	24.25	22.35%	18.79	− 5.21%	25.74	29.86%	28.02	41.35%	44.76	125.84%	**19.82**
	Islamabad	**11.97**	− 0.29%	20.07	67.23%	12.13	1.10%	17.95	49.59%	14.42	20.15%	12.00
	Karachi	8.10	26.61%	15.52	142.71%	8.57	34.05%	15.63	144.38%	7.97	24.61%	**6.3**
	Kolkata	18.70	19.39%	17.30	10.44%	20.24	29.22%	25.51	62.83%	22.88	46.03%	**15.66**
	Lahore	33.07	15.79%	**27.99**	− 2.01%	39.55	38.48%	40.95	43.37%	38.98	36.47%	28.56
	Mumbai	10.59	39.84%	10.60	39.96%	12.56	65.90%	14.66	93.56%	11.43	50.94%	**7.5**
	Peshawar	29.60	76.33%	31.99	90.55%	26.71	59.08%	32.32	92.53%	31.48	87.50%	**16.78**
	Shanghai	3.34	36.59%	2.82	15.24%	3.39	38.88%	3.59	46.81%	3.72	52.06%	**2.44**
	STD	28.640		9.307		11.871		12.755		19.042		**8.017**
MAPE	Beijing	86.50	− 4.58%	113.43	25.12%	89.57	− 1.20%	93.77	3.44%	**81.31**	− 10.3%	90.6
	Chennai	17.23	− 9.99%	17.44	− 8.86%	17.31	− 9.58%	17.87	− 6.62%	**16.36**	− 14.5%	19.13
	Delhi	101.30	447.58%	18.54	0.22%	44.06	138.16%	52.87	185.80%	157.02	748.75%	**18.5**
	Dhaka	25.61	6.09%	**18.66**	− 22.7%	27.06	12.09%	32.41	34.25%	57.07	136.36	24.1
	Islamabad	**24.46**	− 17.9%	41.83	40.41%	24.56	− 17.5%	41.32	38.72%	30.66	2.94	29.78
	Karachi	20.39	18.07%	44.68	158.76%	21.54	24.72%	44.86	159.79%	19.79	14.59%	**17.26**
	Kolkata	22.96	0.34%	**19.73**	− 13.7%	23.12	1.06%	28.81	25.92%	23.45	2.47%	22.88
	Lahore	33.37	− 5.4%	**25.97**	− 26.3%	42.81	21.37%	46.57	32.03%	38.12	8.08%	35.27
	Mumbai	20.77	31.50%	18.71	18.47%	26.48	67.66%	28.53	80.62%	18.64	18.01%	**15.79**
	Peshawar	42.63	49.95%	42.90	50.90%	44.63	56.98%	43.54	53.14%	62.25	118.94%	**28.4**
	Shanghai	14.51	20.94%	12.39	3.25%	14.73	22.77%	15.05	25.39%	14.45	20.39%	**12.00**
	STD	27.877		27.437		**20.218**		20.364		40.517		20.676

Table 9 (continued)

Error	Station	CNN	% imp	BiLSTM	% imp	GRU	% imp	LSTM	% imp	RNN	% imp	Prop-2
MSLE	Beijing	0.21	16.36 %	0.24	37.31%	0.20	13.33%	0.21	18.76%	0.18	3.75%	**0.178**
	Chennai	0.06	8.28%	0.06	1.87%	0.06	5.91%	0.06	9.01%	**0.05**	− 5.1%	0.056
	Delhi	19.42	32507.25%	0.06	6.61%	0.19	225.88%	0.25	317.15%	0.88	1381.25%	**0.059**
	Dhaka	0.11	33.36%	**0.07**	− 12.6%	0.12	35.75%	0.14	61.47%	0.31	258.89%	0.085
	Islamabad	0.11	2.81%	0.31	199.94%	**0.10**	− 0.4%	0.20	96.36%	0.14	30.55%	0.103
	Karachi	0.08	47.12%	0.27	425.01%	0.08	55.34%	0.28	437.62%	0.07	35.23%	**0.051**
	Kolkata	0.11	25.06%	0.09	0.71%	0.11	24.21%	0.15	73.05%	0.11	29.64 %	**0.087**
	Lahore	0.16	12.72%	**0.11**	− 23.5%	0.21	48.92%	0.24	62.79%	0.19	33.92%	0.144
	Mumbai	0.07	60.78%	0.06	37.90%	0.10	120.81%	0.12	172.88%	0.07	49.14%	**0.043**
	Peshawar	0.29	180.97%	0.34	239.14%	0.22	119.14%	0.35	246.60%	0.32	216.83%	**0.101**
	Shanghai	0.03	50.39%	0.03	16.31%	0.04	51.76%	0.04	61.40%	0.03	46.85%	**0.023**
	STD	5.547		0.110		0.060		0.089		0.230		**0.043**

Bold font indicate the best value(s) in row-wise comparision

embassies' datasets. The results demonstrate that the prop-2 model typically outperforms traditional models in terms of MSLE. For example, in Beijing, the prop-2 achieves an MSLE of 0.17, improving over CNN by 16.36% and RNN by 3.75%. In Delhi, the prop-2 model's MSLE of 0.05 represents an extraordinary improvement over CNN by 32,507.25% and RNN by 1,381.25%, highlighting its exceptional performance in this location. Despite a few instances, such as Chennai and Islamabad, where improvements are negative or marginal, the proposed-DR model generally shows lower MSLE values than traditional models. This consistent performance across diverse datasets underscores the robustness and accuracy of the prop-2 in reducing prediction errors see Table 10.

7.1.3 Proposed-2 (1DCNN-BiGRU-DR) Model Versus Traditional Deep Learning with Decompose Recompose

The Table 10 appears to present the performance measures of various models (such as CNN-DR, BiLSTM-DR, GRU-DR, LSTM-DR, RNN-DR, and prop-2 (1DCNN-BiGRU-DR)) on a dataset related to the US embassies dataset. The performance is evaluated using metrics like RMSE, MAE, MAPE, and MSLE for different stations and the percentage improvement (% imp) of each model over the traditional DL decompose-recompose models. The performance improvement of the prop-2 model over the conventional DL decompose-recompose models varies across stations and error metrics.

- **RMSE**: The prop-2 model has a minimum of RMSE 4.18 in Shanghai and a maximum of RMSE 41.91 in Lahore compared to all traditional deep learning-DR overall embassies. The maximum percentage improvement to CNN-DR Delhi was 362.33%, and the minimum percentage improvement to GRU-DR Mumbai was − 0.74% with the RMSE value 13.10035 and prop-2 RMSE value 13.19879 for the same station Mumbai. For example, in the first row under the RMSE error, the CNN-DR model has a value of 12.10949 for the Beijing station, indicating its RMSE performance, with a percentage improvement of 87.04 compared to a baseline. Similarly, the prop-2 model has the lowest RMSE value (6.47) for the Beijing station. For some stations like Delhi, Dhaka, Islamabad, Karachi, Mumbai, and Peshawar, the proposed model exhibits substantial improvements (e.g., percentage improvements range from 0.17% to 9.80%) over other models, suggesting its effectiveness in predicting embassy-related data accurately. The degree of improvement varies across stations and models, indicating that the effectiveness of each model may

Table 10 Performance comparison of deep learning decoposed-recomposed (DL-DR) and proposed-2 deep learning model using RMSE, MAE, MAPE, and MSLE of US Embassies dataset (DL-DR vs. Prop-2)

Error	Station	CNN-DR	% imp	BiLSTM-DR	% imp	GRU-DR	% imp	LSTM-DR	% imp	RNN-DR	% imp	Prop-2
RMSE	Beijing	12.10	87.04%	8.36	29.15%	11.85	83.04%	7.010	8.28%	6.624	2.31%	**6.47**
	Chennai	33.27	318.98%	10.49	32.07%	8.2188	3.48%	10.335	30.13%	7.969	0.34%	**7.94**
	Delhi	120.14	362.33%	31.89	22.73%	26.718	2.81%	27.038	4.04%	26.032	0.17%	**25.98**
	Dhaka	124.46	300.15%	41.54	33.56%	33.512	7.74%	32.822	5.53%	31.292	0.60%	**31.10**
	Islamabad	54.10	223.08%	19.34	15.52%	19.393	15.8%	19.359	15.60%	16.836	0.53%	**16.74**
	Karachi	14.73	29.71%	12.57	10.65%	14.262	25.51%	14.417	26.88%	11.553	1.67%	**11.36**
	Kolkata	39.81	46.4%	30.67	12.79%	28.571	5.05%	28.677	5.44%	**27.085**	− 0.40%	27.19
	Lahore	56.36	34.46%	54.33	29.63%	43.855	4.62%	42.520	1.43%	44.010	4.99%	**41.91**
	Mumbai	28.67	117.24%	14.46	9.61%	**13.100**	− 0.74%	13.333	1.01	13.111	− 0.65%	13.19
	Peshawar	28.39	19.49%	25.76	8.39%	24.100	1.40%	78.017	228.26%	26.097	9.80%	**23.76**
	Shanghai	4.78	14.32%	5.187	23.90%	4.401	5.13%	4.391	4.89%	4.235	1.16%	**4.18**
	STD	40.561		15.342		11.877		21.069		12.354		**11.856**
MAE	Beijing	7.83	126.3%	4.950	42.98%	7.519	117.20%	3.949	14.0%	3.692	6.6%	**3.46**
	Chennai	30.1	524.20%	7.610	57.81%	5.162	7.05%	7.588	57.35%	4.90	1.64%	**4.82**
	Delhi	98.959	626.38%	18.661	36.98%	14.560	6.8%	14.731	8.1%	**13.571**	− 0.3%	13.62
	Dhaka	106.22	435.94%	30.684	54.8%	21.989	10.94%	21.558	8.7%	20.08	1.32%	**19.82**
	Islamabad	47.66	297.18%	15.127	26.05%	15.020	25.16%	15.179	26.49%	12.12	1.03%	**12.00**
	Karachi	10.11	58.10%	7.968	24.61%	9.495	48.50%	9.508	48.7%	**6.333**	− 0.9%	6.39
	Kolkata	27.94	78.39%	19.09	21.87%	16.916	7.98%	16.821	7.38%	**15.450**	− 1.36%	15.66
	Lahore	42.84	49.99%	40.98	43.48%	30.4837	6.72%	28.933	1.2%	30.82	7.9%	**28.56**
	Mumbai	20.15	166.13%	9.460	24.9%	**7.56**	− 0.04%	7.69	1.62%	7.623	0.66%	7.57
	Peshawar	20.45	21.83%	19.09	13.77%	17.115	1.95%	70.562	320.34%	19.316	15.07%	**16.7**
	Shanghai	2.969	21.4%	3.272	33.90%	2.669	9.24%	2.643	8.17%	2.524	3.30%	**2.44**
	STD	34.916		11.525		8.140		19.065		8.637		**8.002**
MAPE	Beijing	120.55	32.9%	122.64	35.28%	99.50	9.75%	106.58	17.56%	99.32	9.5%	**90.65**
	Chennai	100.95	427.46%	27.306	42.67%	21.46	12.13%	29.78	55.61%	19.73	3.13%	**19.1**
	Delhi	97.58	427.45%	28.788	55.60%	20.94	13.21%	21.47	16.06 %	19.36	4.67 %	**18.50**
	Dhaka	99.99	314.1%	35.505	47.05%	28.55	18.28%	27.60	14.33%	24.53	1.63%	**24.14**
	Islamabad	100.16	236.26%	35.867	20.4%	34.68	16.45%	36.32	21.92%	30.51	2.42%	**29.78**
	Karachi	26.61	54.13%	22.674	31.32%	25.16	45.76%	24.34	41.02%	**15.77**	− 8.66%	17.26
	Kolkata	31.21	36.42%	30.245	32.17%	25.94	13.36%	25.87	13.08%	**21.59**	− 5.64%	22.88
	Lahore	49.37	39.99%	49.307	39.79%	39.53	12.08%	37.06	5.02%	38.23	8.39%	**35.27**
	Mumbai	34.04	115.52%	23.077	46.09%	17.38	10.05%	17.730	12.24%	16.94	7.26%	**15.79**
	Peshawar	32.74	15.16%	34.593	21.67%	29.63	4.24%	100.77	254.47%	35.25	24.00%	**28.43**
	Shanghai	14.94	24.48%	17.957	49.62%	13.51	12.64%	13.44	12.0%	12.64	5.34%	**12.00**
	STD	39.065		29.023		23.470		32.242		24.275		**21.700**

Table 10 (continued)

Error	Station	CNN-DR	% imp	BiLSTM-DR	% imp	GRU-DR	% imp	LSTM-DR	% imp	RNN-DR	% imp	Prop-2
MSLE	Beijing	0.352	97.64%	0.276	55.22%	0.306	71.73%	0.223	25.50%	0.202	13.41%	**0.178**
	Chennai	7.443	13188.93%	0.101	81.52%	0.065	17.52 %	0.106	90.15%	0.057	2.69%	**0.056**
	Delhi	10.572	17651.84%	0.107	79.73%	0.067	12.74%	0.070	18.24%	0.061	3.71%	**0.059**
	Dhaka	18.284	21328.45%	0.149	74.8%	0.108	26.7%	0.103	20.83%	0.087	2.06%	**0.085**
	Islamabad	14.305	13657.69%	0.141	36.00%	0.138	33.55%	0.1429	37.50%	0.107	3.34%	**0.103**
	Karachi	0.094	83.94%	0.072	41.37%	0.08	69.00%	0.087	68.92%	**0.049**	− 3.92%	0.051
	Kolkata	0.139	59.88%	0.125	44.11%	0.103	17.96%	0.103	19.02%	**0.082**	− 5.08%	0.087
	Lahore	0.240	66.86%	0.237	64.24%	0.168	16.91%	0.15	7.44 %	0.1608	11.42%	**0.144**
	Mumbai	0.167	280.73%	0.071	62.90%	0.049	12.76%	0.052	18.65%	0.046	7.03%	**0.043**
	Peshawar	0.134	32.53%	0.133	31.81%	0.108	6.62%	10.497	10237.22%	0.1405	38.39%	**0.101**
	Shanghai	0.033	44.45%	0.045	96.31%	0.028	23.09%	0.029	26.74%	0.025	8.10%	**0.023**
	STD	6.802		0.069		0.076		3.133		0.054		**0.045**

Bold font indicate the best value(s) in row-wise comparision

depend on the specific characteristics or patterns present in the data from different embassy stations. Overall, the RMSE analysis suggests that the proposed model offers promising results in predicting the performance measures of US embassies, demonstrating its potential for practical applications in this domain.

- **MAE**: Prop-2 model has a minimum of MAE 2.44 in Shanghai and a maximum of MAE 28.56 in Lahore compared to all traditional deep learning-DR model overall embassies. The maximum percentage improvement to CNN-DR Delhi was 626.38 %, and the minimum percentage improvement to RNN-DR Kolkata was − 1.36% with the MAE value 15.45084 and prop-2 MAE value 15.665277 for the same station Kolkata. For stations like Delhi, Dhaka, Islamabad, Karachi, Mumbai, and Peshawar, the proposed model shows significant improvements over other models, with percentage improvements ranging from 0.34% to 7.90%. Traditional DL models such as BiLSTM-DR, LSTM-DR, and GRU-DR also exhibit competitive performance in some cases. Still, the proposed model consistently outperforms them across various stations regarding MAE. Overall, the MAE analysis suggests that the prop-2 model offers promising results in predicting the performance measures of US embassies, demonstrating its potential for practical applications in this domain, similar to the observations from the RMSE analysis.
- **MAPE**: Comparing the prop-2 model to all traditional DL-DR models across all embassies, the minimum MAPE in Shanghai is 12.00, and the maximum MAPE in Beijing is 90.65. The maximum percentage improvement to CNN-DR Chennai was 427.46 %, and the minimum percentage improvement to RNN-DR Karachi was − 8.66% with the MAPE value of 15.77 and the prop-2 MAPE value of 17.26 for the same station in Karachi. For stations like Delhi, Dhaka, Islamabad, Karachi, Mumbai, and Peshawar, the proposed model shows significant improvements over other models, with percentage improvements ranging from 1.03% to 8.66%. This suggests that the proposed model effectively predicts performance measures for these embassy stations. The prop-2 generally demonstrates competitive or superior performance compared to other models across most stations. It achieves lower MAPE values, indicating better predictive accuracy regarding percentage error.
- **MSLE**: The Prop-2 model has a minimum of MSLE 0.023 in Shanghai and a maximum of MSLE 0.17 in Beijing, compared to all traditional DL-DR models overall embassies. The maximum percentage improvement to CNN-DR Dhaka was 21328.45 %, and the minimum percentage improvement to RNN-DR Kolkata was − 5.08% with the MSLE value 0.082 and prop-2

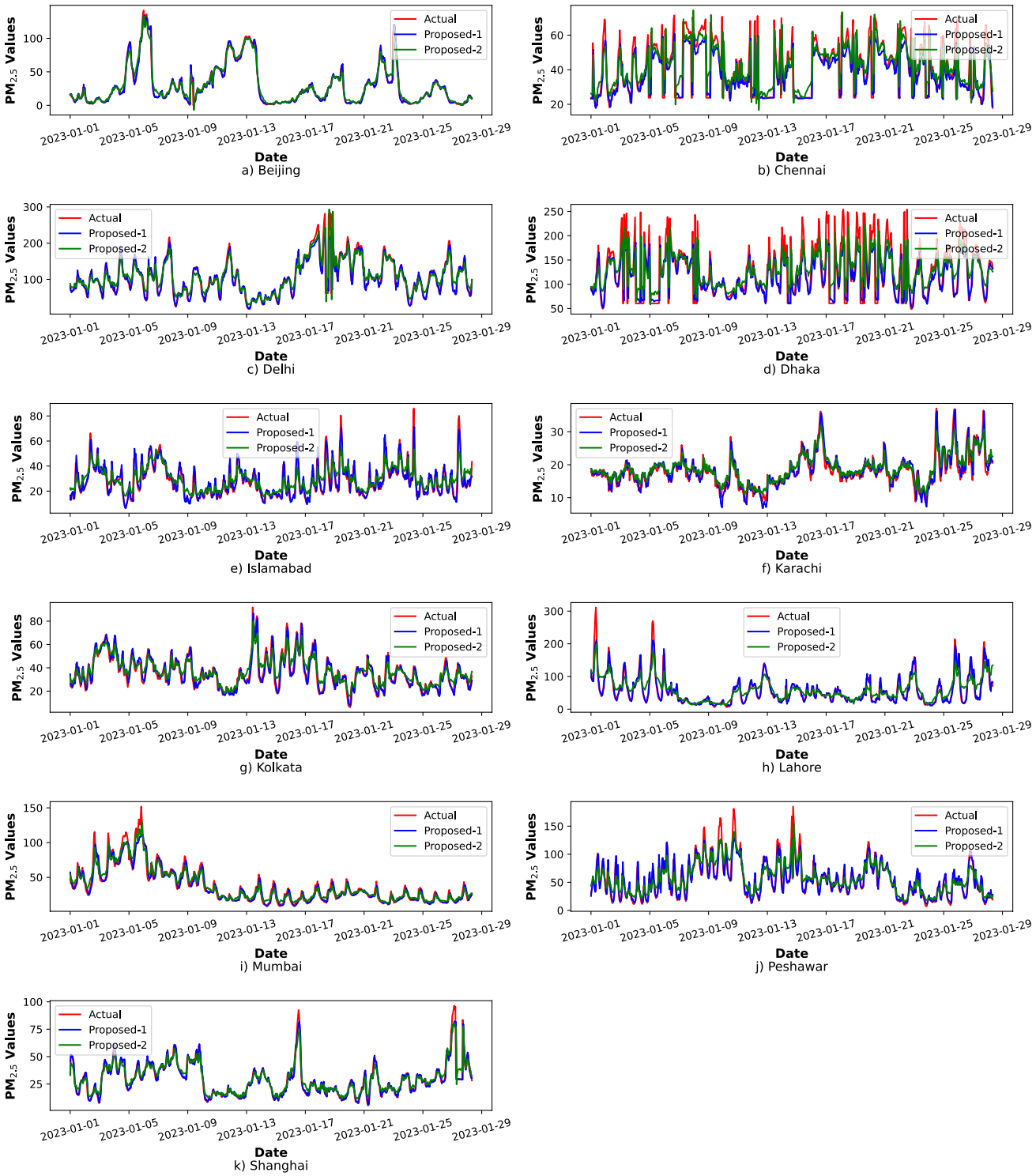

Fig. 6 The line graph of the actual, proposed-1, and proposed-1 model predicted values of $PM_{2.5}$ test set

MSLE value 0.087 for the same station Kolkata. For stations like Delhi, Dhaka, Islamabad, Karachi, Mumbai, and Peshawar, the proposed model shows significant improvements over other models, with percentage improvements ranging from 2.42% to 38.39%. This indicates that the proposed model effectively captures the logarithmic errors, especially for instances with large actual values. Traditional DL models such as BiLSTM-DR, LSTM-DR, and GRU-DR also exhibit competitive performance in some cases. Still, the prop-2

model consistently outperforms them across various stations regarding MSLE.

Prop-2 model consistently demonstrates competitive or superior performance compared to other models, showcasing lower values across all metrics and indicating better predictive accuracy. This superiority is particularly notable for stations like Delhi, Dhaka, Islamabad, Karachi, Mumbai, and Peshawar, where the prop-2 model exhibits significant percentage improvements over other models. While traditional DL models show competitive performance in some cases, the proposed-2 consistently outperforms them across various stations and metrics, emphasizing its effectiveness and potential for practical applications in embassy-related data prediction tasks.

7.2 Graphical Analysis

The predictive pattern of the model over the various datasets is represented in the plots see Sect. 7.2.1. Historical values are displayed alongside predicted values generated by fitting a predictive model to the data. The graph allows for a visual comparison between observed historical patterns and forecasted trends see Fig 6. Historical data points are plotted alongside predicted values obtained using a predictive model. By comparing the observed data distribution with the expected values of prop-1 and prop-2, this graphical approach facilitates an assessment of how well the model captures the overall distribution and trend of the data.

7.2.1 Predictive Pattern Analysis

The line plot in Fig. 6 displays a comprehensive comparison between the observed $PM_{2.5}$ values and the predicted values of the prop-1 and prop-2 models for the test data from 01-01-2023 to 29-01-2023 in all selected US embassies. The line plot shows that the predicted values of the prop-1 and prop-2 models are in close agreement with the actual $PM_{2.5}$ values. Specifically, the prop-2 model closely aligns with the actual values for all cities except for Lahore and Peshawar, where there is a slight deviation from the actual $PM_{2.5}$ values. Similarly, the proposed model closely matches the actual values for all cities except for Chennai and Dhaka, where the proximity to the actual $PM_{2.5}$ values is a bit lower, likely due to the high fluctuation of the actual data.

7.2.2 Predictive Distribution Analysis

The scatter plot in Fig. 7 comparison across 12 cities reveals the performance of two proposed models Prop-1 (gray) and Prop-2 (black) in predicting $PM_{2.5}$ concentrations using the R^2 score. Prop-2 consistently outperforms Prop-1 in 8 cities, with the highest improvement observed in Karachi (0.733 vs. 0.703) and Kolkata (0.744 vs. 0.723). Prop-1 slightly edges out Prop-2 in Delhi (0.877 vs. 0.876) and Lahore (0.742 vs. 0.697), though the difference is marginal. In Peshawar, only Prop-2's score (0.63) is reported, indicating its exclusive use in that city. Overall, Prop-2 demonstrates stronger

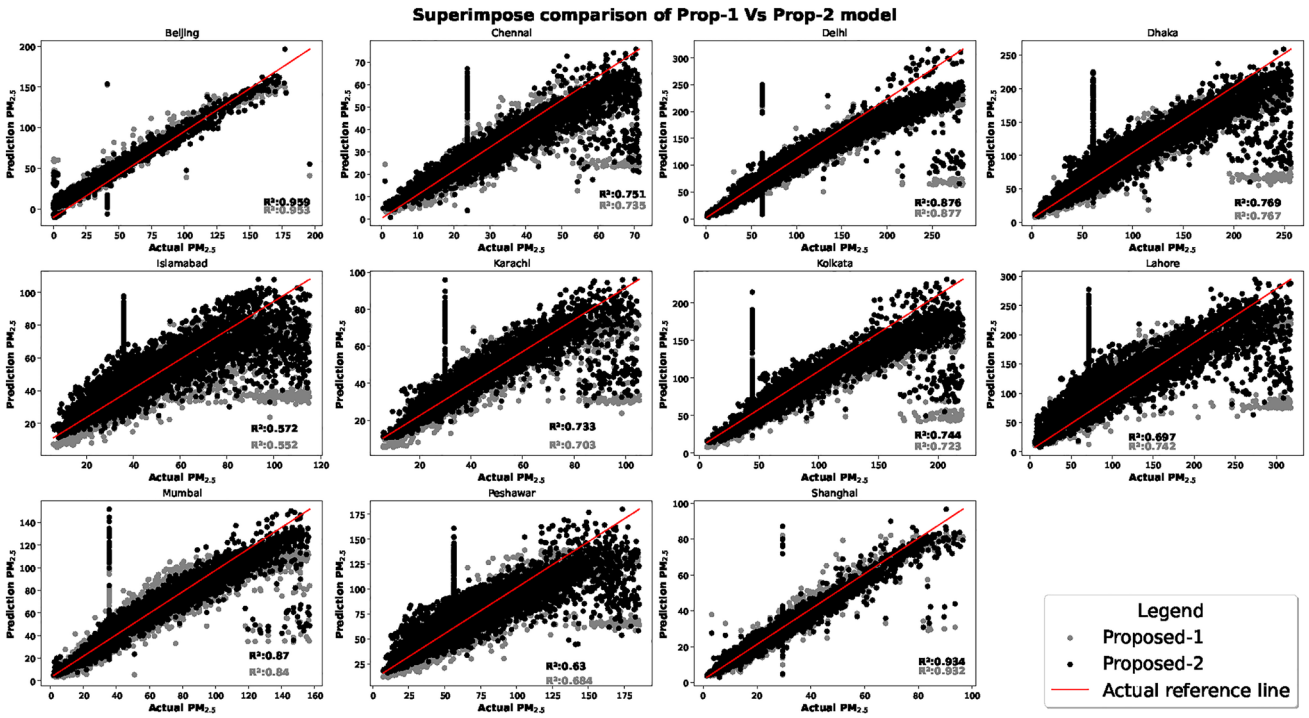

Fig. 7 The superimposed scattered plot of the actual, proposed-1, and proposed-1 model predicted values of $PM_{2.5}$ test set

and more reliable predictive accuracy across diverse urban environments.

7.3 Statistical Analysis of Results Based on Measured Values and Predictions

The non-parametric Friedman ranking test is designed for repeated measures designs, where the same subjects are measured under different conditions. The Friedman rank test provides a robust and flexible ranking method for analyzing models with different conditional parameters. Using AIC and BIC in the context of ARIMA models helps manage the complexity of learning and ensures the selection of models that balance fit. These criteria provide a robust framework for model comparison, allowing analysts to choose models that are not only statistically sound but also practically useful for forecasting and analysis. The difference should exceed ten of the traditional and proposed models regarding the AIC and BIC values. A model is encouraged to explain data effectively while avoiding overfitting by penalizing excessive parameters. The DM test compares the forecast accuracy of two models. It helps identify a more accurate model. The Diebold-Mariano test is crucial for comparing the predictive accuracy of models. A Taylor diagram simultaneously displays three statistical metrics: correlation coefficient, standard deviation, and RMSE. This integration provides a comprehensive view of model performance. It

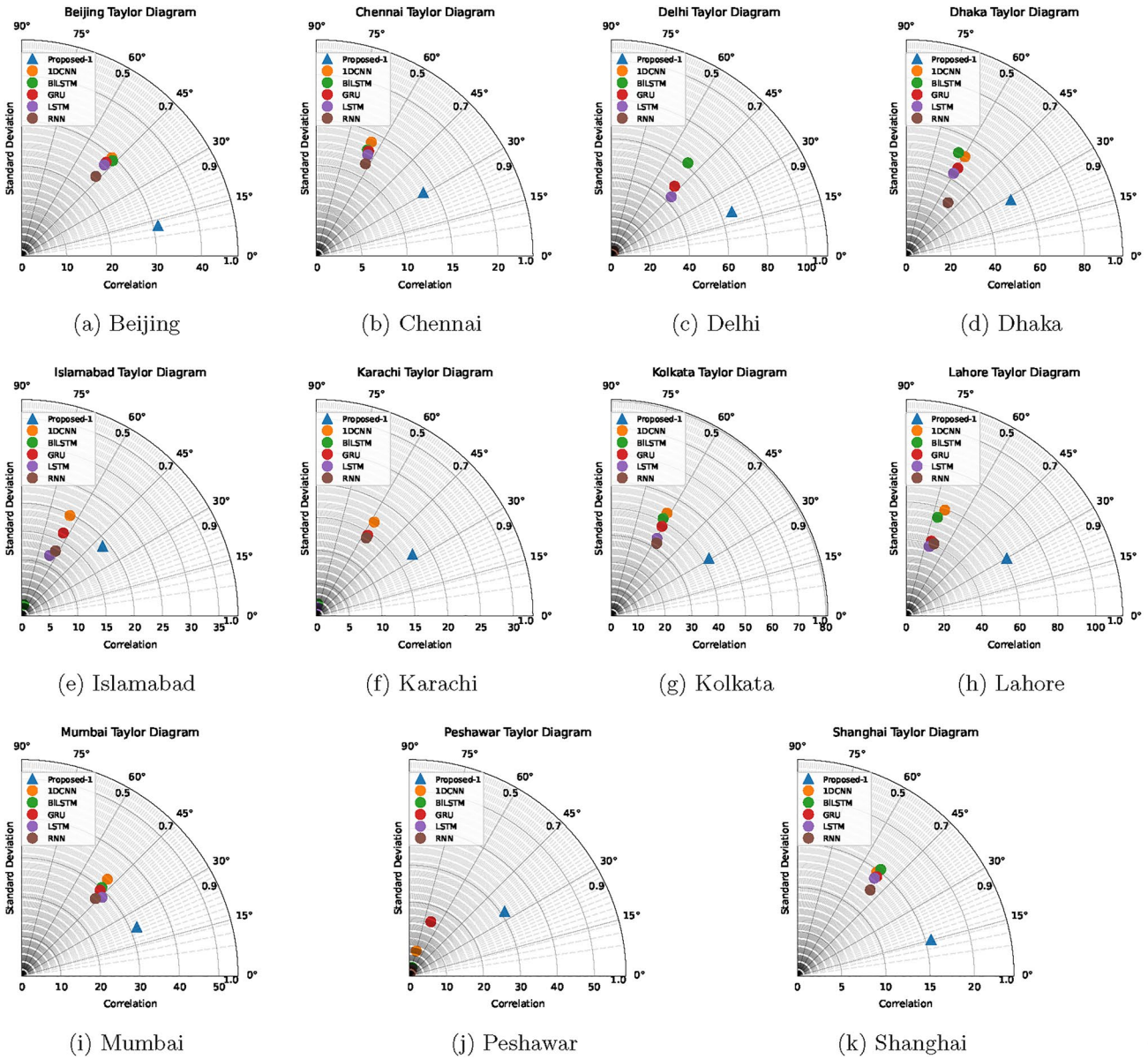

(a) Beijing (b) Chennai (c) Delhi (d) Dhaka

(e) Islamabad (f) Karachi (g) Kolkata (h) Lahore

(i) Mumbai (j) Peshawar (k) Shanghai

Fig. 8 The model's predictive correlation representation using Taylor diagram of prop-1 and traditional models

allows for comparing the performance of various models against a reference.

7.3.1 Taylor Diagram Results Analysis

The statistical importance of apparent discrepancies and the angle to which unforced internal variability and observational uncertainty restrict the predicted agreement between the model and observed behaviors are indicated in these diagrams using Taylor's methodology. This part compares traditional state-of-the-art models with the US Embassy datasets for prop-1 and prop-2 performance indicators. The Taylor diagram is a mathematical graph that compares different approximate representations to see the most realistic visually. The comparison in the Taylor diagram was based on model correlations and root-mean-square deviation when comparing the best predictions to the observed values of $PM_{2.5}$ at various US embassies with different traditional models to the proposed model. Correlation Coefficient is represented as the angle from the horizontal axis Fig. 8. Higher correlations close to one indicate a better match between the observed and modeled data. The radial distance from the origin represents the standard deviation. Close to the origin is the best model. The observed standard deviation is plotted as a circle at a fixed radius. Model standard deviations are compared to this observed value. The prop-1 model demonstrates improved accuracy and consistency compared to traditional models, as indicated by its

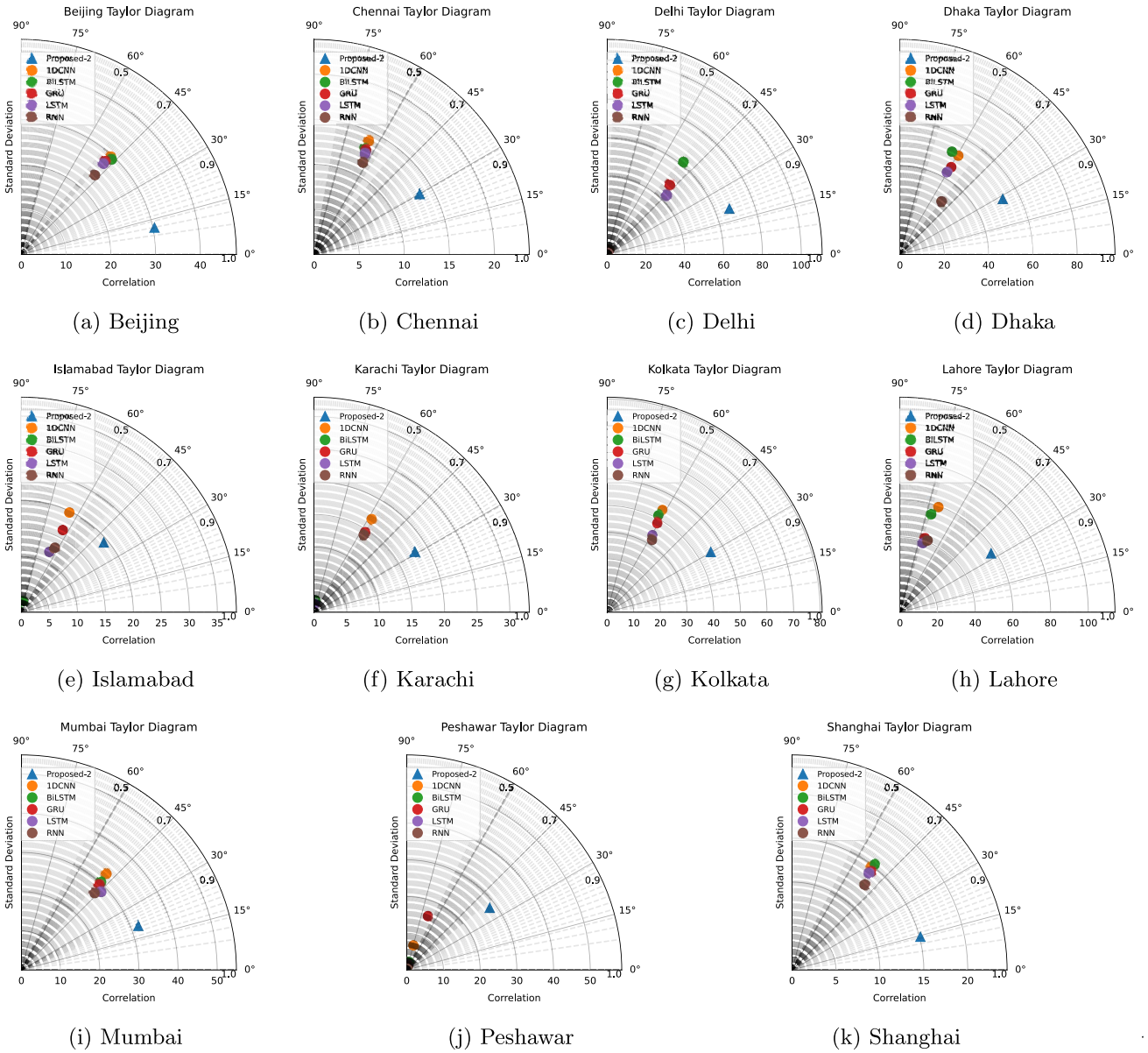

(a) Beijing (b) Chennai (c) Delhi (d) Dhaka

(e) Islamabad (f) Karachi (g) Kolkata (h) Lahore

(i) Mumbai (j) Peshawar (k) Shanghai

Fig. 9 The model's predictive correlation representation using Taylor diagram of prop-2 and traditional models

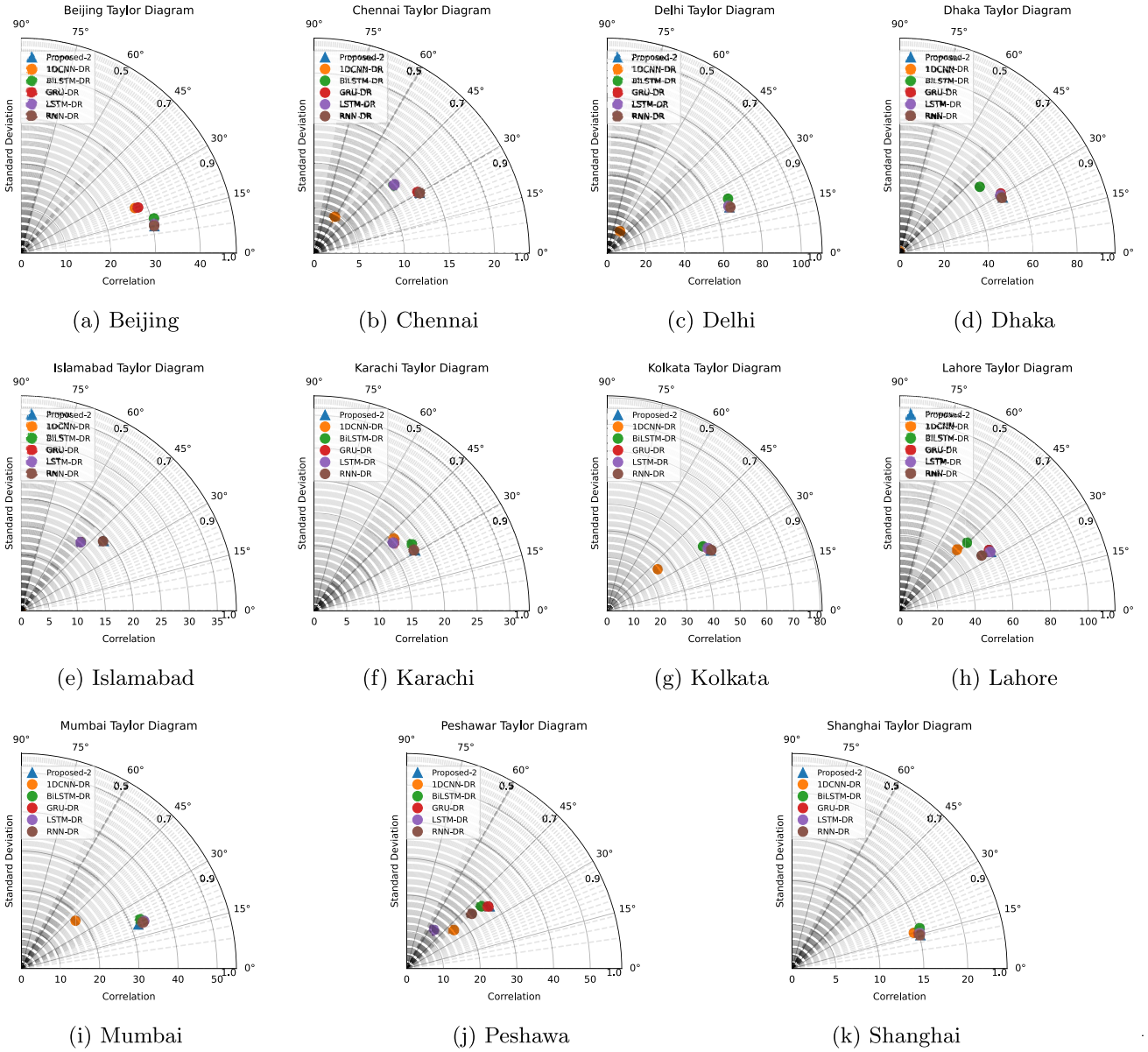

(a) Beijing (b) Chennai (c) Delhi (d) Dhaka

(e) Islamabad (f) Karachi (g) Kolkata (h) Lahore

(i) Mumbai (j) Peshawa (k) Shanghai

Fig. 10 The model's predictive correlation representation using Taylor diagram of prop-2 and DL-DR models

proximity to the reference point. The proposed model correlates highest with the actual Beijing of 0.976 and a standard deviation of 31.048. The proposed model correlates lowest with the actual Islamabad of 0.757 and a standard deviation of 18.992. The prop-1 indicates a high correlation and less standard deviation.

Prop-2 model spans eleven cities: Beijing, Chennai, Delhi, Dhaka, Islamabad, Karachi, Kolkata, Lahore, Mumbai, Peshawar, and Shanghai. Each point on the diagram represents a city's model data, showing the correlation and standard deviation relative to observed data. Correlation values range from approximately 0.76 to 0.98, indicating varying levels of agreement between the model predictions and actual observations, with higher values denoting better correlation. Standard deviation values span from about 13.48 to 67.23, reflecting the differences in variability of the observed data across cities. This diagram effectively illustrates the accuracy and variability of the prop-2 predictions for multiple cities in comprehensive visual Fig. 9. The prop-2 exhibits a robust correlation and a narrow standard deviation.

The Taylor diagram illustrates the statistical relationship between models and observations. The radial distance from the origin represents the standard deviation of the models or observed data, normalized by the standard deviation of the observations. The azimuthal position indicates the correlation coefficient between the model and observations. The correlation coefficient is represented as the angle from

Table 11 Diebold-Mariano test over the predictive values of prop-1 and prop-2 corresponding to traditional model and DL-DR models

	Cities	Vs 1DCNN	Vs BiLSTM	Vs GRU	Vs LSTM	Vs RNN
Prop-1 vs Trad. DL	Beijing	− 21.36275182	− 22.2601457	− 21.32643442	− 21.15288478	− 20.63535641
	Chennai	− 30.25785746	− 30.16662046	− 29.34764165	− 28.83029259	− 28.39023794
	Delhi	− 57.79717459	− 29.16726481	− 28.38137888	− 28.19077167	− 48.76049027
	Dhaka	− 30.6721947	− 33.11531026	− 30.44161478	− 30.73192201	− 27.50740647
	Islamabad	− 22.57609542	− 34.01255992	− 21.0799336	− 23.61979571	− 21.27940055
	Karachi	− 23.34999881	− 31.16320744	− 23.21579461	− 31.388653	− 23.10226934
	Kolkata	− 26.35903746	− 27.14981535	− 25.92992852	− 25.94943374	− 25.20031145
	Lahore	− 35.28008146	− 36.76889469	− 34.61465279	− 34.99517554	− 33.98590299
	Mumbai	− 31.20367785	− 31.23460847	− 29.57718143	− 27.30107549	− 29.56862021
	Peshawar	− 33.60888932	− 35.81442583	− 31.84463698	− 36.0006781	− 38.50200133
	Shanghai	− 25.08302666	− 25.9347781	− 24.82276286	− 24.77699247	− 23.945986
	Cities	Vs 1DCNN	Vs BiLSTM	Vs GRU	Vs LSTM	Vs RNN
Prop-2 vs Trad. DL	Beijing	− 21.68546082	− 22.64327915	− 21.64487457	− 21.47385656	− 20.95558281
	Chennai	− 33.31426014	− 33.40649388	− 32.50853513	− 32.0571209	− 31.70032459
	Delhi	− 57.07136198	− 30.60281773	− 29.68555694	− 29.44681471	− 48.17139896
	Dhaka	− 35.30075154	− 36.81129011	− 34.50074113	− 34.88819139	− 29.77134337
	Islamabad	− 25.36202903	− 30.0182475	− 23.30401264	− 25.20692737	− 22.42529203
	Karachi	− 27.07229526	− 29.99797138	− 26.49196494	− 30.17495827	− 25.8914648
	Kolkata	− 30.24880186	− 30.73741301	− 29.40565783	− 28.7669855	− 27.50182602
	Lahore	− 37.02554283	− 37.85560451	− 34.66135967	− 34.93894342	− 33.75413671
	Mumbai	− 33.10895965	− 32.70830997	− 31.27519524	− 28.9075796	− 30.27910029
	Peshawar	− 30.36998325	− 32.55436614	− 31.09739013	− 32.72641504	− 35.57432503
	Shanghai	− 25.77691161	− 26.66624759	− 25.56101559	− 25.49856411	− 24.67379351
	Cities	Vs 1DCNN-DR	Vs BiLSTM-DR	Vs GRU-DR	Vs LSTM-DR	Prop-2 Vs RNN-DR
Prop-2 vs DL-DR	Beijing	− 17.06503849	− 12.25157339	− 16.37129471	− 8.668950711	− 5.524100896
	Chennai	− 73.08898848	− 16.65544796	− 5.073003999	− 16.26825347	− 2.268454087
	Delhi	− 60.00936505	− 10.03336854	− 3.149897047	− 3.095484946	− 0.640344826
	Dhaka	− 62.07147204	− 22.29025085	− 8.730829021	− 7.573572707	− 2.304427037
	Islamabad	− 64.16658986	− 15.82217303	− 15.41419828	− 15.92402733	− 6.944234268
	Karachi	− 17.31845096	− 8.161697642	− 15.17432671	− 15.35566434	− 4.548431028
	Kolkata	− 22.42661619	− 8.927593174	− 5.494166648	− 5.68289566	1.771745535
	Lahore	− 25.30531901	− 24.02412326	− 9.12469329	− 3.603174959	− 8.325091842
	Mumbai	− 30.7915292	− 5.182765965	1.010018079	− 0.88760501	1.719377572
	Peshawar	− 14.86616862	− 13.70400892	− 3.889469863	− 71.54885569	− 13.83452012
	Shanghai	− 7.524655283	− 8.859255614	− 3.932778264	− 3.399339026	− 2.346863322

the horizontal axis Fig. 10. The distance from the reference point on the x-axis represents the mean-square difference between the models and observations, also normalized by the standard deviation of the observations. The closer a model data point is to the reference point, the better the model performance.

Prop-2 model demonstrates strong performance in Beijing, Delhi, Mumbai, and Shanghai, as evidenced by the high correlation values above 0.9 between prop-2 predictions and observations. Cities like Chennai, Dhaka, Karachi, Kolkata, Lahore, and Peshawar show moderate to high correlations (0.8 - 0.9), indicating reasonable agreement with some discrepancies. Islamabad, with a correlation of 0.7629, reflects the lowest model accuracy. Standard deviation analysis reveals the highest variability in Delhi, Lahore, Dhaka, and Kolkata, suggesting more fluctuating data. At the same time, Shanghai, Chennai, Karachi, and Islamabad exhibit the most minor variability, indicating more consistent datasets. Overall, the prop-2 performs well in most cities, with variability and accuracy varying across different locations.

7.3.2 Diebold-Mariano (DM) Test Analysis

The Table 11 Diebold-Mariano test results reveal that the proposed model significantly outperforms various traditional deep learning models across multiple cities in terms of predictive accuracy. Negative DM statistics indicate a better predictive accuracy of the prop-1 model than traditional models. For instance, the prop-1 model in Delhi shows

substantial improvements with a DM statistic of − 57.80 against 1DCNN, suggesting a noteworthy predictive performance difference. Similar patterns are observed in other cities, such as Karachi and Lahore, where the prop-1 model consistently outperforms the traditional models. The magnitude of these statistics highlights the robustness and superior accuracy of the prop-1 model in diverse urban settings. These findings underscore the potential of the proposed approach in enhancing predictive tasks compared to existing deep learning frameworks. The results of the Diebold-Mariano test indicate that the prop-2 model outperforms traditional deep learning models in terms of predictive accuracy across multiple cities. The negative values across all city comparisons suggest that the prop-2 model has a lower prediction error than the traditional models. Larger negative values indicate a more significant improvement in predictive accuracy by the prop-2 model. For instance, Delhi shows a tremendous negative value of − 57.07136198 when comparing Prop-2 to 1DCNN, indicating a substantial improvement in accuracy. Similarly, large negative values for other cities and models, such as − 37.85560451 for prop-2 vs. BiLSTM in Lahore, further affirm the superior performance of the prop-2 model. Overall, the consistent negative values across all cities and models underscore the effectiveness of the prop-2 model in enhancing predictive accuracy over traditional deep learning models. The Diebold-Mariano test results in the table indicate a consistent outperformance of the prop-2 model over traditional deep learning models with DR across multiple cities. Significant negative DM statistics highlight the superior predictive accuracy of the prop-2 model. The prop-2 model shows substantial improvements in Chennai and Islamabad, with DM statistics of − 73.09 and − 64.17 against 1DCNN-DR, respectively. Similarly, in Delhi and Dhaka, the prop-2 model outperforms with notable margins compared to all traditional models. Interestingly, some cities like Mumbai and Kolkata show less pronounced differences and even some positive values e.g., Mumbai with 1.01 against GRU-DR, suggesting comparable performance or a slight edge over traditional models in a few cases. However, overall, the data underscores the robustness and enhanced predictive capability of the prop-2 model in most urban city environments, affirming its effectiveness in improving forecast accuracy through advanced DR techniques.

The Diebold-Mariano test allows for a direct statistical comparison of the forecast accuracy of two models, which helps determine which model provides more accurate forecasts. Rather than evaluating models in isolation, the DM test assesses their relative performance, clarifying which model is better. The analysis of the Table 11 test supports better model selection, development, and validation practices by providing a clear and statistical comparison. The superior performance of the prop-1 and prop-2 models is evident.

7.3.3 AIC and BIC Test

The Table 12 presents the AIC and BIC test values for traditional deep learning models versus the prop-1 model across various cities, demonstrating the comparative model fit. For each model-city pair, both AIC and BIC scores are significantly lower for the proposed models than traditional models, with differences ranging from several thousand to over ten thousand points. For instance, in Beijing, the AIC and BIC differences for the 1DCNN model are 12481.69, indicating a substantial improvement in model fit with the prop-1 model. Similar trends are observed across cities like Delhi and Shanghai, where the prop-1 model outperforms traditional models by large margins in AIC and BIC metrics. This consistent reduction in both AIC and BIC values suggests that the prop-1 model better fits the data, indicating its superior predictive accuracy and efficiency compared to traditional deep learning approaches.

The Table 13 provides a descriptive analysis of the AIC and BIC scores for traditional deep learning models compared to the prop-2 model across different cities. The diff column represents the difference between the AIC and BIC scores of the traditional and prop-2 models. Generally, the positive differences indicate that the AIC and BIC scores are notably lower for each city for the prop-2 model than the conventional models. The suggested model offers a better fit for the data across all cities, with substantial improvements in model fit observed consistently. For example, in Beijing, the AIC and BIC differences for the 1DCNN model are 13136.41, indicating a significant enhancement in model fit with the prop-2 model. Similar trends are observed across other cities, reaffirming the superiority of the prop-2 model in terms of model fit and predictive accuracy compared to traditional deep learning approaches.

The Table 14 presents a comparative analysis of traditional deep learning models with DR like 1DCNN-DR, BiLSTM-DR, GRU-DR, LSTM-DR, RNN-DR against prop-2 models using AIC and BIC scores across multiple cities. Positive differences in AIC and BIC scores between the traditional and prop-2 indicate an enhancement in the model that fits the proposed approach. In contrast, less than ten or negative differences suggest better performance of traditional models. The findings indicate that the prop-2 technique improves model fit and predictive accuracy across diverse cities, as evidenced by positive differences in most cases, highlighting the efficacy of the prop-2 approach in enhancing model performance.

The models selected based on the AIC BIC test are presented as potential options for evaluating the effectiveness

Table 12 AIC and BIC test over the predictive values of the traditional vs prop-1 model

City	Model	Trad. AIC	AIC Prop-1	diff	Trad. BIC	BIC Prop-1	diff
Beijing	1DCNN	31324.01	18842.31	**12,481.69**	31356.46	18874.77	**12,481.69**
	BiLSTM	31065.99	18842.31	**12,223.67**	31098.44	18874.77	**12,223.67**
	GRU	31241.45	18842.31	**12,399.14**	31273.9	18874.77	**12,399.14**
	LSTM	31126.65	18842.31	**12,284.34**	31159.1	18874.77	**12,284.34**
	RNN	30834.29	18842.31	**11,991.97**	30866.74	18874.77	**11,991.97**
Chennai	1DCNN	27005.81	20472.21	**6533.6**	27038.26	20504.66	**6533.6**
	BiLSTM	26768.55	20472.21	**6296.336**	26,801	20504.66	**6296.336**
	GRU	26679.8	20472.21	**6207.583**	26712.25	20504.66	**6207.583**
	LSTM	26532.15	20472.21	**6059.94**	26564.6	20504.66	**6059.94**
	RNN	26230.71	20472.21	**5758.496**	26263.16	20504.66	**5758.496**
Delhi	1DCNN	47170.3	31665.17	**15,505.13**	47202.75	31697.62	**15,505.13**
	BiLSTM	39701.77	31665.17	**8036.603**	39734.22	31697.62	**8036.603**
	GRU	39039.21	31665.17	**7374.042**	39071.66	31697.62	**7374.042**
	LSTM	38750.14	31665.17	**7084.977**	38782.59	31697.62	**7084.977**
	RNN	41774.28	31665.17	**10,109.12**	41806.73	31697.62	**10,109.12**
Dhaka	1DCNN	39724.86	33503.96	**6220.905**	39757.31	33536.41	**6220.905**
	BiLSTM	40216.3	33503.96	**6712.343**	40248.75	33536.41	**6712.343**
	GRU	39483.95	33503.96	**5979.991**	39516.4	33536.41	**5979.991**
	LSTM	39420.66	33503.96	**5916.701**	39453.11	33536.41	**5916.701**
	RNN	38549.58	33503.96	**5045.618**	38582.03	33536.41	**5045.618**
Islamabad	1DCNN	31234.55	27658.63	**3575.92**	31,267	27691.08	**3575.92**
	BiLSTM	32650.53	27658.63	**4991.897**	32682.98	27691.08	**4991.897**
	GRU	30805.63	27658.63	**3146.999**	30838.08	27691.08	**3146.999**
	LSTM	30802.81	27658.63	**3144.179**	30835.26	27691.08	**3144.179**
	RNN	30606.34	27658.63	**2947.706**	30638.79	27691.08	**2947.706**
Karachi	1DCNN	28892.56	24178.71	**4713.845**	28925.01	24211.16	**4713.845**
	BiLSTM	30298.54	24178.71	**6119.829**	30330.99	24211.16	**6119.829**
	GRU	28575.08	24178.71	**4396.363**	28607.53	24211.16	**4396.363**
	LSTM	30360.23	24178.71	**6181.518**	30392.68	24211.16	**6181.518**
	RNN	28522.82	24178.71	**4344.106**	28555.27	24211.16	**4344.106**
Kolkata	1DCNN	38260.41	32549.43	**5710.989**	38292.86	32581.88	**5710.989**
	BiLSTM	38167.14	32549.43	**5617.714**	38199.59	32581.88	**5617.714**
	GRU	37879.43	32549.43	**5330.004**	37911.88	32581.88	**5330.004**
	LSTM	37723.2	32549.43	**5173.775**	37755.65	32581.88	**5173.775**
	RNN	37536.1	32549.43	**4986.674**	37568.55	32581.88	**4986.674**
Lahore	1DCNN	42564.33	35582.19	**6982.141**	42596.78	35614.64	**6982.141**
	BiLSTM	42587.3	35582.19	**7005.111**	42619.75	35614.64	**7005.111**
	GRU	42031.41	35582.19	**6449.228**	42063.86	35614.64	**6449.228**
	LSTM	41953.74	35582.19	**6371.554**	41986.19	35614.64	**6371.554**
	RNN	41869.31	35582.19	**6287.127**	41901.76	35614.64	**6287.127**
Mumbai	1DCNN	32678.78	26134.79	**6543.989**	32711.23	26167.24	**6543.989**
	BiLSTM	32387.32	26134.79	**6252.534**	32419.77	26167.24	**6252.534**
	GRU	32260.89	26134.79	**6126.098**	32293.34	26167.24	**6126.098**
	LSTM	31762.34	26134.79	**5627.549**	31794.79	26167.24	**5627.549**
	RNN	32163.9	26134.79	**6029.109**	32196.35	26167.24	**6029.109**
Peshawar	1DCNN	36336.47	30075.6	**6260.867**	36368.92	30108.05	**6260.867**
	BiLSTM	37128.42	30075.6	**7052.817**	37160.87	30108.05	**7052.817**
	GRU	35043.47	30075.6	**4967.87**	35075.92	30108.05	**4967.87**
	LSTM	37174.11	30075.6	**7098.503**	37206.56	30108.05	**7098.503**
	RNN	35578.68	30075.6	**5503.079**	35611.13	30108.05	**5503.079**
Shanghai	1DCNN	25611.41	14130.8	**11,480.61**	25643.86	14163.25	**11,480.61**
	BiLSTM	25616.44	14130.8	**11,485.64**	25648.89	14163.25	**11,485.64**
	GRU	25293.48	14130.8	**11,162.68**	25325.93	14163.25	**11,162.68**
	LSTM	25316.55	14130.8	**11,185.75**	25,349	14163.25	**11,185.75**
	RNN	24771.22	14130.8	**10,640.42**	24803.67	14163.25	**10,640.42**

Bold font indicate the best value(s) in row-wise comparision

Table 13 AIC and BIC test over the predictive values of the traditional vs prop-2 model

City	Model	Trad. AIC	AIC Prop-2	diff	Trad. BIC	BIC Prop-2	diff
Beijing	1DCNN	31324.01	18187.6	**13,136.41**	31356.46	18220.05	**13,136.41**
	BiLSTM	31065.99	18187.6	**12,878.39**	31098.44	18220.05	**12,878.39**
	GRU	31241.45	18187.6	**13,053.85**	31273.9	18220.05	**13,053.85**
	LSTM	31126.65	18187.6	**12,939.05**	31159.1	18220.05	**12,939.05**
	RNN	30834.29	18187.6	**12,646.69**	30866.74	18220.05	**12,646.69**
Chennai	1DCNN	27005.81	20176.7	**6829.118**	27038.26	20209.15	**6829.118**
	BiLSTM	26768.55	20176.7	**6591.853**	26,801	20209.15	**6591.853**
	GRU	26679.8	20176.7	**6503.1**	26712.25	20209.15	**6503.1**
	LSTM	26532.15	20176.7	**6355.457**	26564.6	20209.15	**6355.457**
	RNN	26230.71	20176.7	**6054.013**	26263.16	20209.15	**6054.013**
Delhi	1DCNN	47170.3	31712.7	**15,457.6**	47202.75	31745.15	**15,457.6**
	BiLSTM	39701.77	31712.7	**7989.074**	39734.22	31745.15	**7989.074**
	GRU	39039.21	31712.7	**7326.513**	39071.66	31745.15	**7326.513**
	LSTM	38750.14	31712.7	**7037.447**	38782.59	31745.15	**7037.447**
	RNN	41774.28	31712.7	**10,061.59**	41806.73	31745.15	**10,061.59**
Dhaka	1DCNN	39724.86	33461.8	**6263.06**	39757.31	33494.25	**6263.06**
	BiLSTM	40216.3	33461.8	**6754.499**	40248.75	33494.25	**6754.499**
	GRU	39483.95	33461.8	**6022.147**	39516.4	33494.25	**6022.147**
	LSTM	39420.66	33461.8	**5958.856**	39453.11	33494.25	**5958.856**
	RNN	38549.58	33461.8	**5087.774**	38582.03	33494.25	**5087.774**
Islamabad	1DCNN	31234.55	27436.77	**3797.784**	31,267	27469.22	**3797.784**
	BiLSTM	32650.53	27436.77	**5213.761**	32682.98	27469.22	**5213.761**
	GRU	30805.63	27436.77	**3368.863**	30838.08	27469.22	**3368.863**
	LSTM	30802.81	27436.77	**3366.043**	30835.26	27469.22	**3366.043**
	RNN	30606.34	27436.77	**3169.57**	30638.79	27469.22	**3169.57**
Karachi	1DCNN	28892.56	23662.03	**5230.524**	28925.01	23694.48	**5230.524**
	BiLSTM	30298.54	23662.03	**6636.508**	30330.99	23694.48	**6636.508**
	GRU	28575.08	23662.03	**4913.042**	28607.53	23694.48	**4913.042**
	LSTM	30360.23	23662.03	**6698.198**	30392.68	23694.48	**6698.198**
	RNN	28522.82	23662.03	**4860.785**	28555.27	23694.48	**4860.785**
Kolkata	1DCNN	38260.41	32155.44	**6104.978**	38292.86	32187.89	**6104.978**
	BiLSTM	38167.14	32155.44	**6011.704**	38199.59	32187.89	**6011.704**
	GRU	37879.43	32155.44	**5723.993**	37911.88	32187.89	**5723.993**
	LSTM	37723.2	32155.44	**5567.765**	37755.65	32187.89	**5567.765**
	RNN	37536.1	32155.44	**5380.663**	37568.55	32187.89	**5380.663**
Lahore	1DCNN	42564.33	36365.69	**6198.637**	42596.78	36398.14	**6198.637**
	BiLSTM	42587.3	36365.69	**6221.607**	42619.75	36398.14	**6221.607**
	GRU	42031.41	36365.69	**5665.724**	42063.86	36398.14	**5665.724**
	LSTM	41953.74	36365.69	**5588.05**	41986.19	36398.14	**5588.05**
	RNN	41869.31	36365.69	**5503.623**	41901.76	36398.14	**5503.623**
Mumbai	1DCNN	32678.78	25119.76	**7559.013**	32711.23	25152.21	**7559.013**
	BiLSTM	32387.32	25119.76	**7267.558**	32419.77	25152.21	**7267.558**
	GRU	32260.89	25119.76	**7141.122**	32293.34	25152.21	**7141.122**
	LSTM	31762.34	25119.76	**6642.573**	31794.79	25152.21	**6642.573**
	RNN	32163.9	25119.76	**7044.133**	32196.35	25152.21	**7044.133**
Peshawar	1DCNN	36336.47	30843.71	**5492.758**	36368.92	30876.16	**5492.758**
	BiLSTM	37128.42	30843.71	**6284.708**	37160.87	30876.16	**6284.708**
	GRU	35043.47	30843.71	**4199.761**	35075.92	30876.16	**4199.761**
	LSTM	37174.11	30843.71	**6330.395**	37206.56	30876.16	**6330.395**
	RNN	35578.68	30843.71	**4734.97**	35611.13	30876.16	**4734.97**
Shanghai	1DCNN	25611.41	13945.57	**11,665.83**	25643.86	13978.02	**11,665.83**
	BiLSTM	25616.44	13945.57	**11,670.87**	25648.89	13978.02	**11,670.87**
	GRU	25293.48	13945.57	**11,347.91**	25325.93	13978.02	**11,347.91**
	LSTM	25316.55	13945.57	**11,370.98**	25,349	13978.02	**11,370.98**
	RNN	24771.22	13945.57	**10,825.65**	24803.67	13978.02	**10,825.65**

Bold font indicate the best value(s) in row-wise comparision

Table 14 AIC and BIC test over the predictive values of the DL-DR vs prop-2

City	Model	Trad. AIC	AIC Prop-2	diff	Trad. BIC	BIC Prop-2	diff
Beijing	1DCNN-DR	24281.5	18187.60037	**6093.903**	24313.95	18220.0505	**6093.903**
	BiLSTM-DR	20677.71	18187.60037	**2490.109**	20710.16	18220.0505	**2490.109**
	GRU-DR	24071.22	18187.60037	**5883.617**	24103.67	18220.0505	**5883.617**
	LSTM-DR	18962.14	18187.60037	**774.5395**	18994.59	18220.0505	**774.5395**
	RNN-DR	18410.55	18187.60037	**222.9467**	18,443	18220.0505	**222.9467**
Chennai	1DCNN-DR	34119.39	20176.6971	**13,942.69**	34151.84	20209.1472	**13,942.69**
	BiLSTM-DR	22884.47	20176.6971	**2707.776**	22916.92	20209.1472	**2707.776**
	GRU-DR	20509.73	20176.6971	**333.0374**	20542.18	20209.1472	**333.0374**
	LSTM-DR	22740.2	20176.6971	**2563.504**	22772.65	20209.1472	**2563.504**
	RNN-DR	20209.93	20176.6971	**33.2349**	20242.38	20209.1472	**33.2349**
Delhi	1DCNN-DR	46613.54	31712.69619	**14,900.84**	46645.99	31745.1463	**14,900.84**
	BiLSTM-DR	33706.04	31712.69619	**1993.343**	33738.49	31745.1463	**1993.343**
	GRU-DR	31982.97	31712.69619	**270.2777**	32015.42	31745.1463	**270.2777**
	LSTM-DR	32098.91	31712.69619	**386.2174**	32131.36	31745.1463	**386.2174**
	RNN-DR	31729.81	31712.69619	**17.11,748**	31762.26	31745.1463	**17.11,748**
Dhaka	1DCNN-DR	46957.05	33461.80428	**13,495.24**	46989.5	33494.2544	**13,495.24**
	BiLSTM-DR	36278.29	33461.80428	**2816.487**	36310.74	33494.2544	**2816.487**
	GRU-DR	34187.92	33461.80428	**726.114**	34220.37	33494.2544	**726.114**
	LSTM-DR	33985.64	33461.80428	**523.8386**	34018.09	33494.2544	**523.8386**
	RNN-DR	33520.98	33461.80428	**59.17,323**	33553.43	33494.2544	**59.17,323**
Islamabad	1DCNN-DR	38849.93	27436.76969	**11,413.16**	38882.38	27469.2198	**11,413.16**
	BiLSTM-DR	28841.67	27436.76969	**1404.903**	28874.12	27469.2198	**1404.903**
	GRU-DR	28864.74	27436.76969	**1427.972**	28897.19	27469.2198	**1427.972**
	LSTM-DR	28847.81	27436.76969	**1411.043**	28880.26	27469.2198	**1411.043**
	RNN-DR	27488.81	27436.76969	**52.04,219**	27521.26	27469.2198	**52.04,219**
Karachi	1DCNN-DR	26194.34	23662.03411	**2532.31**	26226.79	23694.4842	**2532.31**
	BiLSTM-DR	24647.76	23662.03411	**985.7265**	24680.21	23694.4842	**985.7265**
	GRU-DR	25874.06	23662.03411	**2212.022**	25906.51	23694.4842	**2212.022**
	LSTM-DR	25979.02	23662.03411	**2316.991**	26011.47	23694.4842	**2316.991**
	RNN-DR	23823.84	23662.03411	**161.807**	23856.29	23694.4842	**161.807**
Kolkata	1DCNN-DR	35865.84	32155.43607	**3710.402**	35898.29	32187.8862	**3710.402**
	BiLSTM-DR	33326.86	32155.43607	**1171.425**	33359.31	32187.8862	**1171.425**
	GRU-DR	32635.68	32155.43607	**480.2441**	32668.13	32187.8862	**480.2441**
	LSTM-DR	32671.64	32155.43607	**516.2012**	32704.09	32187.8862	**516.2012**
	RNN-DR	32115.92	32155.43607	− 39.5126	32148.37	32187.8862	− 39.5126
Lahore	1DCNN-DR	39247.54	36365.69032	**2881.854**	39279.99	36398.1405	**2881.854**
	BiLSTM-DR	38891.49	36365.69032	**2525.795**	38923.94	36398.1405	**2525.795**
	GRU-DR	36805.64	36365.69032	**439.9496**	36838.09	36398.1405	**439.9496**
	LSTM-DR	36504.79	36365.69032	**139.0991**	36537.24	36398.1405	**139.0991**
	RNN-DR	36839.97	36365.69032	**474.2751**	36872.42	36398.1405	**474.2751**
Mumbai	1DCNN-DR	32670.34	25119.76293	**7550.582**	32702.8	25152.2131	**7550.582**
	BiLSTM-DR	26012.98	25119.76293	**893.2201**	26045.43	25152.2131	**893.2201**
	GRU-DR	25046.92	25119.76293	− 72.8409	25079.37	25152.2131	− 72.8409
	LSTM-DR	25218.44	25119.76293	**98.67,293**	25250.89	25152.2131	**98.67,293**
	RNN-DR	25055.44	25119.76293	− 64.3261	25087.89	25152.2131	− 64.3261
Peshawar	1DCNN-DR	32576.73	30843.71124	**1733.019**	32609.18	30876.1614	**1733.019**
	BiLSTM-DR	31627.99	30843.71124	**784.2767**	31660.44	30876.1614	**784.2767**
	GRU-DR	30979.33	30843.71124	**135.6214**	31011.78	30876.1614	**135.6214**
	LSTM-DR	42411.71	30843.71124	**11,568**	42444.16	30876.1614	**11,568**
	RNN-DR	31754.25	30843.71124	**910.5409**	31786.7	30876.1614	**910.5409**
Shanghai	1DCNN-DR	15248.75	13945.57249	**1303.181**	15281.2	13978.0226	**1303.181**
	BiLSTM-DR	16031.94	13945.57249	**2086.37**	16064.39	13978.0226	**2086.37**
	GRU-DR	14432.78	13945.57249	**487.2067**	14465.23	13978.0226	**487.2067**
	RNN-DR	14058.52	13945.57249	**112.9465**	14090.97	13978.0226	**112.9465**

Bold font indicate the best value(s) in row-wise comparision

Table 15 Post Hoc Comparison Table for $\alpha = 0.05$ (FRIEDMAN) RMSE, MAE, MAPE, and MSLE

Models	RMSE			MAE			MAPE			MSLE		
	Rank	p value	p_{Holm}	Rank	p value	p_{Holm}	Rank	p value	p_{Holm}	Rank	p value	p_{Holm}
LSTM	5.45	0	0	5.36	0	0	5.36	0	0.000001	5.54	0	0
RNN	4.72	0.000003	0.000012	4.72	0.000003	0.000012	3.72	0.001418	0.004255	3.63	0.00095	0.002851
GRU	3.45	0.002091	0.006274	3.81	0.000411	0.001234	4.18	0.000169	0.000678	3.63	0.00095	0.002851
1DCNN	3.45	0.002091	0.006274	3	0.000411	0.001234	3.09	0.016703	0.016703	3.81	0.000411	0.001645
BiLSTM	2.9	0.016703	0.016703	3.09	0.008765	0.01753	3.45	0.004385	0.008771	3.36	0.003047	0.003047
Proposed-1	1	–	–	1	–	–	1.18	–	–	1	–	–
LSTM	5.45	0	0	5.36	0	0.000001	5.27	0.000169	0.000847	5.54	0	0.000001
RNN	4.72	0.000003	0.000012	4.72	0.000015	0.00006	3.63	0.087375	0.262126	3.54	0.006237	0.018711
GRU	3.45	0.002091	0.006274	3.81	0.001418	0.004255	3.9	0.040239	0.160955	3.54	0.006237	0.018711
1DCNN	3.45	0.002091	0.006274	2.9	0.040239	0.080477	2.81	0.494125	0.610118	3.81	0.002091	0.008366
BiLSTM	2.9	0.016703	0.016703	2.9	0.040239	0.080477	3.09	0.305059	0.610118	3.18	0.022654	0.022654
Proposed-2	1	–	–	1.27	–	–	2.27	–	–	1.36	–	–
1DCNN-DR	5.81	0	0	5.81	0	0	5.54	0	0	5.72	0	0
BiLSTM-DR	4.45	0.000066	0.000266	4.54	0.000066	0.000266	4.54	0.000009	0.000035	4.45	0.000041	0.000163
LSTM-DR	3.81	0.001418	0.004255	3.81	0.002091	0.006274	3.9	0.000629	0.001887	4	0.000411	0.001234
GRU-DR	3.36	0.008765	0.01753	3.27	0.016703	0.033407	3.45	0.004385	0.008771	3.45	0.004385	0.008771
RNN-DR	2.27	0.21	0.21	2.18	0.305059	0.305059	2.18	0.21	0.21	2.18	0.21	0.21
Proposed-2	1.27	–	–	1.36	–	–	1.18	–	–	1.18	–	–

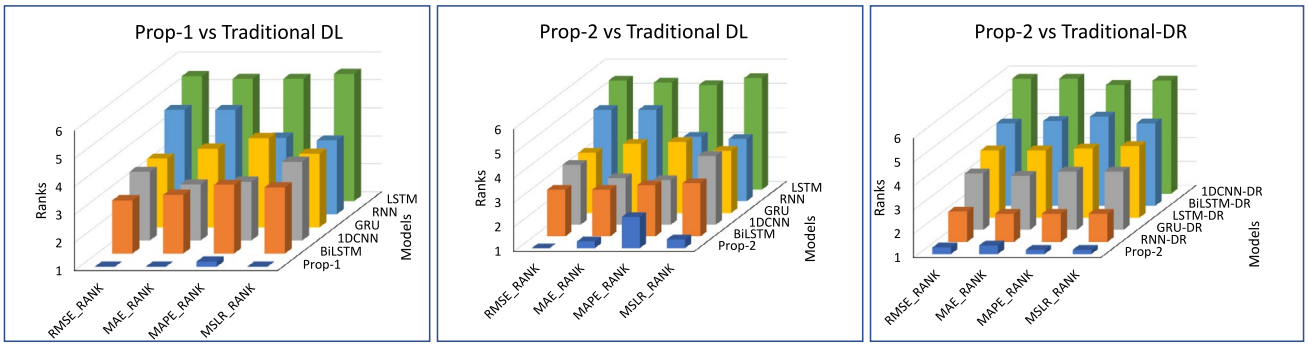

Fig. 11 The rankings of the proposed models compared to deep learning models with respect to the various evaluation parameters

of different models and finding the most suitable model from the selection. After carefully examining the AIC BIC test, it is clear that the suggested models outperform all other traditional models and DL-DR models. The superiority of the proposed models is confirmed through a thorough comparison and evaluation process

7.3.4 Non-parametric Statistical Friedman Ranking

The Friedman process results were subjected to post hoc procedures to obtain the p-values. Holm's sequential rejective technique outlined that hypotheses presenting an unadjusted p-value of ≤ 0.016667 for RMSE, ≤ 0.025 for MAE, ≤ 0.05 for MAPE, and ≤ 0.025 for MSLE were deemed invalid. Based on the Friedman procedure results, the p-values were acquired using post hoc techniques.

The Table 15 post hoc comparison table presents p-values obtained through Holm's procedure applied over the results of the Friedman test for different error metrics: RMSE, MAE, MAPE, and MSLE. Holm's method controls the family-wise error rate and determines which models show statistically significant differences in performance. For RMSE, Holm's procedure rejects hypotheses with unadjusted p-values ≤ 0.016667. Models such as 1DCNN-DR, LSTM, RNN, GRU, 1DCNN, BiLSTM, BiLSTM-DR, and LSTM-DR show significant results, with the highest adjusted p-value being 0.0125 for LSTM-DR. For MAE, Holm's threshold i ≤ 0.025, with significant models including 1DCNN-DR, LSTM, RNN, GRU, 1DCNN, BiLSTM, BiLSTM-DR, LSTM-DR, and GRU-DR, all showing adjusted p-values under this threshold. For MAPE, Holm's procedure rejects hypotheses with p-values ≤ 0.05. All models except RNN-DR and the proposed models demonstrate significant differences, with the highest significant adjusted p-value being 0.016667 for BiLSTM. For MSLE, Holm's procedure rejects hypotheses with unadjusted p-values ≤ 0.025. Considerable models include 1DCNN-DR, LSTM, RNN, GRU, 1DCNN, BiLSTM, BiLSTM-DR, LSTM-DR, and GRU-DR, with adjusted p-values up to 0.0125 for GRU-DR. The rank of the RMSE shows that the prop-1 and prop-2 models are given the best rank among all traditional deep learning models. Three distinct analytical approaches are pursued: prop-1 vs. DL, prop-2 vs. DL, and prop-2 vs. DL-DR. The ranking of the prop-1 model compared to traditional models based on RMSE values reveals that the prop-1 model achieved the top position, followed by BiLSTM in second place, 1DCNN in third place, and so forth. Similarly, comparing RMSE rankings between prop-2 and traditional models shows that the prop-2 model secured the first position, with BiLSTM ranking second, and so on. Moreover, when examining the RMSE ranking of prop-2 compared to DL-DR models, the prop-2 model excelled in the first position with a value of 1.27. In contrast, RNN-DR and GRU-DR attained the second and third ranks with values of 2.27 and 3.36, respectively, and so forth Fig. 11.

8 Conclusion

Our study introduces a new method to improve the $PM_{2.5}$ prediction accuracy, which involves combining a hybrid 1DCNN-BiGRU model with the decompose-recompose 1DCNN-BiGRU-DR methodology. By utilizing the strengths of deep learning architectures and advanced data preprocessing techniques, authors have shown significant enhancements in $PM_{2.5}$ forecasting accuracy compared to traditional methods, with different analyses of the test results. The authors employed publicly accessible data sourced from AirNow US embassies and consulates situated in the Indian subcontinent and China to assess and contrast the predictive capacity of the suggested model against several cutting-edge benchmark models. Extensive experiments use real-world $PM_{2.5}$ datasets from various United States embassy locations. Our model's outstanding performance, as indicated by evaluation metrics such as MAE, RMSE, and R^2, highlights its ability to capture the complex spatio-temporal patterns inherent in $PM_{2.5}$ data. Validating the test results of the prop-1 and prop-2 models against the different

statistical and non-statistical parameters and graphical analysis. The proposed framework is compared to conventional deep learning techniques to evaluate a range of parameter metrics, encompassing statistical and non-statistical indicators and graphical examinations. Three distinct analytical approaches are pursued: prop-1 vs. DL, prop-2 vs. DL, and prop-2 vs. DL-DR. The ranking of the prop-1 model compared to traditional models based on RMSE values reveals that the prop-1 model achieved the top position, followed by BiLSTM in second place, 1DCNN in third place, and so forth. Similarly, comparing RMSE rankings between prop-2 and traditional models shows that the prop-2 model secured the first position, with BiLSTM ranking second, and so on. Moreover, when examining the RMSE ranking of prop-2 compared to DL-DR models, the prop-2 model excelled in the first position with a value of 1.27. In contrast, RNN-DR and GRU-DR attained the second and third ranks with values of 2.27 and 3.36, respectively, and so forth. Our research has real-world implications for public health and environmental policy beyond advancing air quality forecasting techniques. Future research could advance the integration and adaptive application of seasonal and trend decomposition using loss, Unobserved component models, Hodrick-Prescott filter, and Singular Spectrum Analysis methods in time series analysis. This involves investigating their combined effectiveness in capturing complex patterns, developing adaptive versions that automatically adjust to varying data characteristics, and conducting robustness checks across domains.

Author Contributions Naushad Ahmad: Conceptualization of this study, Methodology, Writing - Methodology, Software, Data curation, Writing - Original draft preparation, Visualization, Writing - Review. Vipin Kumar: Validation, Formal analysis, Methodology, Investigation, Editing, Supervision.

Funding No funding was received for conducting this study.

Data Availability The datasets (https://www.airnow.gov/) and code generated or analyzed during the current study are available from the corresponding author on reasonable request. Availability of GIS data: Download data by country for arcgis plot (https://www.diva-gis.org/).

Code Availability All code was implemented in Python. Interested researchers can request access by contacting the corresponding author.

Declarations

Conflict of interest The authors have no Conflict of interest to declare.

Ethical Approval and Consent to Participate Not applicable. https://diva-gis.org/data.html

Consent for Publication Not applicable

References

Ahmad N, Kumar V (2023) A hybrid time series model for the spatio-temporal analysis of air pollution prediction based on pm 2.5. In: International conference on advanced network technologies and intelligent computing, pp. 62–81. https://doi.org/10.1007/978-3-031-64067-4_5 . Springer

Ahmad N, Kumar V (2025) Enhancing pm 2.5 air pollution forecasting with novel random imputation based on hybrid rnn-bidirectional gru (nri rnn-bigru) model. SN Comput Sci 6(6):637. https://doi.org/10.1007/s42979-025-04167-y

Ahmad N, Kumar V (2025) Spatio-temporal forecasting using a hybrid bigru-1dcnn model for pm 2.5 concentrations in Delhi, India (2018-2023) across multiple monitoring stations. Water Air Soil Pollut 236(7):459. https://doi.org/10.1007/s11270-025-08103-x

Bi J, Knowland KE, Keller CA, Liu Y (2022) Combining machine learning and numerical simulation for high-resolution pm 2. 5 concentration forecast. Environ Sci Technol 56(3):1544–1556. https://doi.org/10.1021/acs.est.1c05578

Bai W, Li F (2023) Pm2.5 concentration prediction using deep learning in internet of things air monitoring system. Environ Eng Res. https://doi.org/10.4491/eer.2021.456

Bilal M, Mhawish A, Nichol JE, Qiu Z, Nazeer M, Ali MA, Leeuw G, Levy RC, Wang Y, Chen Y et al (2021) Air pollution scenario over Pakistan: characterization and ranking of extremely polluted cities using long-term concentrations of aerosols and trace gases. Remote Sens Environ 264:112617. https://doi.org/10.1021/acs.est.1c01863

Buya S, Usanavasin S, Gokon H, Karnjana J (2023) An estimation of daily pm2. 5 concentration in Thailand using satellite data at 1-kilometer resolution. Sustainability 15(13):10024. https://doi.org/10.3390/su151310024

Cebrián AC, Asín J, Gelfand AE, Schliep EM, Castillo-Mateo J, Beamonte MA, Abaurrea J (2022) Spatio-temporal analysis of the extent of an extreme heat event. Stoch Env Res Risk Assess 36(9):2737–2751

Chen M-H, Chen Y-C, Chou T-Y, Ning F-S (2023) Pm2. 5 concentration prediction model: a cnn-rf ensemble framework. Int J Environ Res Public Health 20(5):4077. https://doi.org/10.54097/ajst.v5i3.7347

Chen Y, Huang L, Xie X, Liu Z, Hu J (2024) Improved prediction of hourly pm2. 5 concentrations with a long short-term memory and spatio-temporal causal convolutional network deep learning model. Sci Total Environ 912:168672. https://doi.org/10.1016/j.scitotenv.2023.168672

Chen X, Kong P, Jiang P, Wu Y (2021) Estimation of pm2. 5 concentration using deep Bayesian model considering spatial multiscale. Remote Sens 13(22):4545. https://doi.org/10.3390/rs13224545

Conibear L, Reddington CL, Silver BJ, Chen Y, Knote C, Arnold SR, Spracklen DV (2022) Sensitivity of air pollution exposure and disease burden to emission changes in china using machine learning emulation. GeoHealth 6(6):2021–000570. https://doi.org/10.1029/2021GH000570

Chae S, Shin J, Kwon S, Lee S, Kang S, Lee D (2021) Pm10 and pm2. 5 real-time prediction models using an interpolated convolutional neural network. Sci Rep 11(1):11952. https://doi.org/10.1038/s41598-021-91253-9

Choi H-S, Song K, Kang M, Kim Y, Lee K-K, Choi H (2022) Deep learning algorithms for prediction of pm10 dynamics in urban and rural areas of Korea. Earth Sci Inf 15(2):845–853. https://doi.org/10.1007/s12145-022-00771-1

Duan Y, Li H, He M, Zhao D (2021) A Bigru autoencoder remaining useful life prediction scheme with attention mechanism and skip connection. IEEE Sens J 21(9):10905–10914. https://doi.org/10.1109/JSEN.2021.3060395

Du S, Li T, Yang Y, Horng S-J (2019) Deep air quality forecasting using hybrid deep learning framework. IEEE Trans Knowl Data Eng 33(6):2412–2424. https://doi.org/10.1109/TKDE.2019.2954510

Geng G, Xiao Q, Liu S, Liu X, Cheng J, Zheng Y, Xue T, Tong D, Zheng B, Peng Y et al (2021) Tracking air pollution in china: near real-time pm2. 5 retrievals from multisource data fusion. Environ Sci Technol 55(17):12106–12115. https://doi.org/10.1021/acs.est.1c01863

Hu W, Fang L, Zhang H, Ni R, Pan G (2023) Changing trends in the air pollution-related disease burden from 1990 to 2019 and its predicted level in 25 years. Environ Sci Pollut Res 30(1):1761–1773. https://doi.org/10.1007/s11356-022-22318-z

Hari Prasad Peri S (2023) Short-term exposure to air pollution and covid-19 in India: spatio-temporal analysis of relative risk from 20 metropolitan cities. Spat Inf Res 31(4):1–14

Hickmann T, Widerberg O, Lederer M, Pattberg P (2021) The united nations framework convention on climate change secretariat as an orchestrator in global climate policymaking. Int Rev Adm Sci 87(1):21–38. https://doi.org/10.1177/0020852319840425

Hu J, Zhou R, Ding R, Ye D-W, Su Y (2023) Effect of pm2. 5 air pollution on the global burden of lower respiratory infections, 1990–2019: a systematic analysis from the global burden of disease study 2019. J Hazard Mater 459:132215

Islam MS, Roy S, Tusher TR, Rahman M, Harris RC (2023) Assessing spatio-temporal variations in pm2. 5 pollution and associated mortality in the south Asian region. Available at SSRN 4392794

Kotsev A, Peeters O, Smits P, Grothe M (2015) Building bridges: experiences and lessons learned from the implementation of inspire and e-reporting of air quality data in europe. Earth Sci Inf 8:353–365. https://doi.org/10.1007/s12145-014-0160-8

Khanam Z, Sultana FM, Mushtaq F (2023) Environmental pollution control measures and strategies: an overview of recent developments. Geospatial Anal Environ Pollution Model Anal Control Manag. https://doi.org/10.1007/978-3-031-45300-7_15

Li X, Huo H (2023) Prediction of pm2. 5 concentration based on cnn-bigru model. Acad J Sci Technol 5(3):1–8. https://doi.org/10.3390/ijerph20054077

Li L (2020) A robust deep learning approach for spatiotemporal estimation of satellite aod and pm2. 5. Remote Sens 12(2):264. https://doi.org/10.3390/rs12020264

Limperis J, Tong W, Hamza-Lup F, Li L (2023) Pm 2.5 forecasting based on transformer neural network and data embedding. Earth Sci Inform 16(3):2111–2124. https://doi.org/10.1007/s12145-023-01002-x

Mohan AS, Abraham L (2024) An ensemble deep learning approach for air quality estimation in Delhi, India. Earth Sci Inform 17(3):1–26. https://doi.org/10.1007/s12145-023-01210-5

Mohammadi F, Teiri H, Hajizadeh Y, Abdolahnejad A, Ebrahimi A (2024) Prediction of atmospheric pm2. 5 level by machine learning techniques in Isfahan, Iran. Sci Rep 14(1):2109. https://doi.org/10.1038/s41598-024-52617-z

Nair AS, Khare S, Thakur A (2023) Air quality index prediction of bangalore city using various machine learning methods. In: Information and communication technology for competitive strategies (ICTCS 2022) intelligent strategies for ICT, pp. 391–406. Springer. https://doi.org/10.1007/978-981-19-9304-6_37

Natarajan SK, Shanmurthy P, Arockiam D, Balusamy B, Selvarajan S (2024) Optimized machine learning model for air quality index prediction in major cities in India. Sci Rep 14(1):6795. https://doi.org/10.1038/s41598-024-54807-1

Prasad KV, Vaidya H, Rajashekhar C, Karekal KS, Sali R (2023) Automated neural network forecast of pm concentration. Int J Math Comput Eng 1(1):67–78. https://doi.org/10.2478/ijmce-2023-0005

Qing L (2023) Pm2. 5 concentration prediction using gra-gru network in air monitoring. Sustainability 15(3):1973. https://doi.org/10.3390/su15031973

Raza WA, Mahmud I, Rabie TS (2022) Breathing heavy: new evidence on air pollution and health in Bangladesh, 1st edn. World Bank development in practice series, vol. 25. World Bank Publications, Washington, DC. https://doi.org/10.1596/978-1-4648-1919-3

Stafoggia M, Bellander T, Bucci S, Davoli M, De Hoogh K, De'Donato F, Gariazzo C, Lyapustin A, Michelozzi P, Renzi M et al (2019) Estimation of daily pm10 and pm2. 5 concentrations in Italy, 2013–2015, using a spatiotemporal land-use random-forest model. Environ Int 124:170–179. https://doi.org/10.1016/j.envint.2019.01.016

Shakya D, Deshpande V, Agarwal M (2022) A deep learning based model to predict pm concentration. In: 2022 IEEE 4th international conference on cybernetics, cognition and machine learning applications (ICCCMLA), pp. 286–291. https://doi.org/10.1109/ICCCMLA56841.2022.9989071 . IEEE

Samad A, Garuda S, Vogt U, Yang B (2023) Air pollution prediction using machine learning techniques-an approach to replace existing monitoring stations with virtual monitoring stations. Atmos Environ 310:119987. https://doi.org/10.1016/j.atmosenv.2023.119987

Shekdar AV (2009) Sustainable solid waste management: an integrated approach for Asian countries. Waste Manage 29(4):1438–1448. https://doi.org/10.1016/j.wasman.2008.08.025

Shao X, Kim CS (2022) Accurate multi-site daily-ahead multi-step pm 25 concentrations forecasting using space-shared cnn-lstm. Comput Mater Continua https://doi.org/10.32604/cmc.2022.020689

Sethi JK, Mittal M (2021) An efficient correlation based adaptive lasso regression method for air quality index prediction. Earth Sci Inf 14(4):1777–1786. https://doi.org/10.1007/s12145-021-00618-1

Shewalkar A, Nyavanandi D, Ludwig SA (2019) Performance evaluation of deep neural networks applied to speech recognition: Rnn, lstm and gru. J. Artif Intell Soft Comput Res 9(4):235–245. https://doi.org/10.2478/jaiscr-2019-0006

Samal KKR, Panda AK, Babu KS, Das SK (2021) An improved pollution forecasting model with meteorological impact using multiple imputation and fine-tuning approach. Sustain Cities Soc 70:102923. https://doi.org/10.1016/j.scs.2021.102923

Sahoo AK, Pradhan C, Das H (2020) Performance evaluation of different machine learning methods and deep-learning based convolutional neural network for health decision making. Nat Inspired Comput Data Sci. https://doi.org/10.1007/978-3-030-33820-6_8

Sharma K, Tiwari R, Wadhwani AK, Chaturvedi S (2024) Spatiotemporal analysis of land surface temperature trends in Nashik, India: a 30-year study from 1992 to 2022. Earth Sci Inform 17(3):1–22. https://doi.org/10.1007/s12145-024-01260-3

Sun X, Tian Z, Zhang Z (2023) A new decomposition-integrated air quality index prediction model. Earth Sci Inf 16(3):2307–2321. https://doi.org/10.1007/s12145-023-01028-1

Toharudin T, Caraka RE, Pratiwi IR, Kim Y, Gio PU, Sakti AD, Noh M, Nugraha FAL, Pontoh RS, Putri TH et al (2023) Boosting algorithm to handle unbalanced classification of pm2.5 concentration levels by observing meteorological parameters in Jakarta-Indonesia using adaboost, xgboost, catboost, and lightgbm. IEEE Access. https://doi.org/10.1109/ACCESS.2023.3265019

Vignesh PP, Jiang JH, Kishore P (2023) Predicting pm2. 5 concentrations across USA using machine learning. Earth Space Sci 10(10):2023–002911. https://doi.org/10.1029/2023EA002911

Wang W, Mao W, Tong X, Xu G (2021) A novel recursive model based on a convolutional long short-term memory neural network for air pollution prediction. Remote Sens 13(7):1284. https://doi.org/10.3390/rs13071284

Wu Y, Song P, Lin S, Peng L, Li Y, Deng Y, Deng X, Lou W, Yang S, Zheng Y et al (2021) Global burden of respiratory diseases attributable to ambient particulate matter pollution: findings from the global burden of disease study 2019. Front Public Health 9:740800. https://doi.org/10.3389/fpubh.2021.740800

Wu X, Wen Q, Zhu J (2023) An ensemble model for pm2. 5 concentration prediction based on feature selection and two-layer clustering algorithm. Atmosphere 14(10):1482. https://doi.org/10.3390/atmos14101482

Wang F, Yao S, Luo H, Huang B (2022) Estimating high-resolution pm2. 5 concentrations by fusing satellite aod and smartphone photographs using a convolutional neural network and ensemble learning. Remote Sens 14(6):1515. https://doi.org/10.3390/rs14061515

Wu X, Zhang C, Zhu J, Zhang X (2022) Research on pm2. 5 concentration prediction based on the ce-aga-lstm model. Appl Sci 12(14):7009. https://doi.org/10.3390/app12147009

Xie Y, Chen X, Zhang L (2023) Prediction of pm2. 5 concentration based on cnnlstm deep learning model. In: 2023 Asia-Europe Conference on Electronics, Data Processing and Informatics (ACEDPI), pp. 229–233. https://doi.org/10.1109/ACEDPI58926.2023.00051 . IEEE

Xiao F, Yang M, Fan H, Fan G, Al-Qaness MA (2020) An improved deep learning model for predicting daily pm2. 5 concentration. Sci Rep 10(1):20988. https://doi.org/10.1038/s41598-020-77757-w

Yu Y, Liu C, Zhou J, Zheng L, Shan X, He L, Zhang L, Guo J, Luo B (2024) Global burden study of lower respiratory infections linked to low temperatures: an analysis from 1990 to 2019. Environ Sci Pollut Res 31(7):1–14. https://doi.org/10.1007/s11356-023-31587-1

Yang X, Xiao D, Bai H, Tang J, Wang W (2022) Spatiotemporal distributions of pm2. 5 concentrations in the Beijing–Tianjin–Hebei region from 2013 to 2020. Front Environ Sci 10:842237. https://doi.org/10.3389/fenvs.2022.842237

Zamani Joharestani M, Cao C, Ni X, Bashir B, Talebiesfandarani S (2019) Pm2. 5 prediction based on random forest, xgboost, and deep learning using multisource remote sensing data. Atmosphere 10(7):373. https://doi.org/10.3390/atmos10070373

Zhang L, Ji Y, Liu T, Li J (2020) Pm2. 5 prediction based on xgboost. In: 2020 7th international conference on information science and control engineering (ICISCE), pp. 1011–1014. https://doi.org/10.1109/ICISCE50968.2020.00207 . IEEE

Zhou R-X, Liao H-J, Hu J-J, Xiong H, Cai X-Y, Ye D-W (2024) Global burden of lung cancer attributable to household fine particulate matter pollution in 204 countries and territories, 1990–2019. J Thorac Oncol. https://doi.org/10.1007/s11356-022-22318-z

Zhu Y, Shi Y (2023) Spatio-temporal variations of pm2. 5 concentrations and related premature deaths in Asia, Africa, and Europe from 2000 to 2018. Environ Impact Assess Rev 99:107046